Geophysical Journal International

Geophys. J. Int. (2020) **220,** 1023–1044
Advance Access publication 2019 October 30
GJI Geomagnetism, rock magnetism and palaeomagnetism

doi: 10.1093/gji/ggz492

New archaeomagnetic secular variation data from Central Europe. I: directions

Elisabeth Schnepp,[1] Daniele Thallner,[1,*] Patrick Arneitz,[2] Hermann Mauritsch,[1] Robert Scholger,[1] Christian Rolf[3] and Roman Leonhardt[2]

[1] *Palaeomagnetic Laboratory Gams, Chair of Geophysics, Montanuniversität Leoben, Gams* 45, *A*8130 *Frohnleiten, Austria.*
E-mail: elisabeth.schnepp@unileoben.ac.at
[2] *ZAMG, Hohe Warte* 38, *A*1190 *Vienna, Austria*
[3] *Leibniz Institute for Applied Geophysics (LIAG), Stilleweg* 2, *D*-30655 *Hannover, Germany*

Accepted 2019 October 28. Received 2019 October 21; in original form 2019 February 25

SUMMARY

Archaeomagnetic directions of 141 archaeological structures have been studied from 21 sites in Austria, 31 sites in Germany and one site in Switzerland. Characteristic remanent magnetization directions obtained from alternating field and thermal demagnetizations provided 82 and 78 new or updated (12 and 10 per cent) directions of Austria and Germany, respectively. Nine of the directions are not reliable for certain reasons (e.g. displacement) while three of the features are not well dated. Apart from this some updated age information for the published databases is provided. Rock magnetic experiments revealed magnetite as main magnetic carrier of the remanences. The new data agree well with existing secular variation reference curves. The extended data set covers now the past 3500 yr and a lot of progress were made to cover times BC with data. Here enhanced secular variation is observed manifested in declinations with values up to 70°. The new data will allow for recalculation of archaeomagnetic calibration curves for Central Europe from mid Bronze Age until today.

Key words: Europe; Archaeomagnetism; Palaeomagnetic secular variation.

1 INTRODUCTION

Palaeomagnetic secular variation (SV) data obtained from archaeological artefacts help to understand the Earth's magnetic field of the past several millennia. They are also used as a dating tool in archaeology as, for an archaeological structure of unknown age, its magnetic direction can be compared with the local SV curve to determine the time at which such magnetization was acquired. The worldwide database of archaeomagnetic and volcanic secular variation data (e.g. Brown *et al.* 2015, Arneitz *et al.* 2017b, and references therein) is steadily expanding and comprises currently 4779 entries for declination and inclination for the past 3500 yr although only few data published after 2014 were taken into account. The data can be used to calculate regional (e.g. Hervé *et al.* 2013; Cai *et al.* 2016) or global calibration curves (e.g. Korte *et al.* 2011; Pavón-Carrasco *et al.* 2014; Arneitz *et al.* 2019) which can be used as reference curves for dating.

Directional archaeomagnetic reference curves have been published for Austria (Schnepp & Lanos 2006) and Germany (Schnepp & Lanos 2005) more than a decade ago. At that time the Austrian calibration curve was based mainly on archaeomagnetic directions from sites outside of Austria, situated in Bosnia, France, Germany, Hungary and Switzerland (for references see table 1 in Schnepp & Lanos 2006). Even though the determined archaeomagnetic directions, especially for Austria, meanwhile cover the past 3500 yr, the Austrian calibration curve has only been updated with some data from the Early Medieval (Schnepp *et al.* 2015) so far. The collection of new data for Germany was concentrated on time intervals with only sparse data coverage and is now also extended back to 1200 BC.

Some of the 'new' data were already published mainly in German or Austrian archaeological journals and monographs which are not easily accessible to the international community. The purpose of the present paper is to supply the catalogues of Austrian and German data with all new or updated archaeomagnetic directions that greatly improve the temporal and spatial data coverage of both countries and compare the new and revised data to the secular variation curves of Central Europe.

* now at: Geomagnetism Laboratory, School of Environmental Sciences, University of Liverpool, L69 7ZE, UK

2 ARCHAEOLOGICAL SITES AND SAMPLING

Although terms like site, sample or specimen have already been introduced, for example by Tarling (1971) the definition in archaeomagnetism is not always clear (see Poletti *et al.* 2018) because it cannot be easily transferred. In this paper, the term 'site' is used for a location where one or an array of archaeological excavations have been performed. At a site (multilevel site) the excavation unearthed one (several or many) archaeological features of *in situ* heated material called 'structure'. Each structure may be accompanied by an archaeological age estimate based on finds related to the structure or by natural science dating, but sometimes such an age exists only for the site or larger features, for example a house in which an oven was found. Each structure is sampled with a number of independently oriented samples. Depending on the sampling technique these samples may be divided into two or more specimens, which are finally subjected to the laboratory measurements. For calculation of the mean direction of a structure the hierarchical levels defined by Lanos *et al.* 2005 were used. In some cases, two or several structures of a site were combined to group with a single mean direction when they had been attributed with the same archaeological age and provided insignificant differences of their archaeomagnetic directions (see below).

Approximately 170 archaeological structures have been sampled at 53 archaeological sites in Austria, Germany and Switzerland (Fig. 1). The kinds of structures listed in Table S1 (SupplementaryMaterialsA) can be attributed to five groups. About one quarter of the structures have been found at metallurgical sites, where iron or copper smelting, metal working or charcoal production took place. Accordingly, structures found at these sites were charcoal piles, roasting pits, smelting furnaces, smith's hearths, a bell mould or single fire setting, used to break up the ore by heat. About 15 per cent of the structures had other technical purposes like brick, glass, lime, or pottery production. Forty per cent of the structures were domestic fires like bread ovens or hearths, or structures that were used to heat buildings like praefurnia, hypocausts or firesides. The rest of the structures were burnt soils, floors or walls due the incendiary fires (∼8 per cent) or ovens of unknown use (∼10 per cent).

According to the wide range of different structures sampling comprised also many materials, although the majority of samples were baked clay, soil or brick material which are normally used for archaeomagnetic investigations. In addition, the samples also comprised slag from metal production, *in situ* sediments or local rocks like granite, gneiss, schist, sandstone, greywacke, limestone or dolomite which were burnt in situ or used as building material for houses and ovens.

Sampling for archaeomagnetic investigations has been conducted using mainly a modified version of the Thellier technique (Thellier 1938) by encasing the baked clay into plaster with a plane surface for orientation and the soft core technique (Schnepp *et al.* 2008). In some cases, *in situ* drilled cores have also been taken using an electrical or gasoline powered drill with diamond bit, and plastic boxes have been used for sampling of soft material (see Table S1, SupplementaryMaterialsA). For a few sites the 'English' technique (e.g. Clark *et al.* 1988; Trapanese *et al.* 2008) has been used. Here the orientation surface is fabricated by a nylon disc (in our case an acryl or glass plate), which is directly glued onto the burnt rock or clay surface.

In order to establish archaeomagnetic dating in Austria sampling comprised all available sites offered by archaeologists. For Germany sampling was concentrated to time intervals which are sparsely covered by the archaeomagnetic database. The temporal distributions (Fig. 2) of the calibration curve data sets for Germany and Austria (Schnepp & Lanos 2005, 2006) show concentrations in the Roman epoch and medieval times. Sampling of new sites in Germany was mainly restricted to sites from times before the 13th century AD but dating requests also provided younger sites. The age intervals of new sites are shown in comparison with the cumulative age distributions of the German and Austrian calibration curves. They show that most of the new sites fill gaps in these temporal distributions and that there is a considerable number of sites dating BC, where the database is still particularly poor for Austria. The geographic distribution of the new sites is shown in Fig. 1. Austria is now also covered with sites, but in Germany a concentration of sites in the northern part and the Rhineland is still present.

With respect to published 22 Austrian and 163 German archaeomagnetic directions (Schnepp & Lanos 2005, 2006; Aidona *et al.* 2006; Trapanese *et al.* 2008; Schnepp *et al.* 2015, 2016; Schnepp & Brüggler 2016) a total of 44 new sites have been sampled and at seven Austrian sites sampling has been continued. The results gave 58 new directions for Austria and 63 for Germany. One site from Switzerland is also included. In addition to Table S1 (SupplementaryMaterialsA) some more information on each archaeological location is given in SupplementaryMaterialsB and below for selected sites. Further information on the archaeological background and/or important stratigraphic relations can be found in publications in archaeological media which also provided the preliminary results (Klemm *et al.* 2005; Schnepp 2008a, b, 2010a, b, 2011a, b, 2015, 2016, 2017, 2018; Klemm *et al*. 2017).

2.1 MULTILEVEL SITES

The majority of sites provided more than one feature often with different ages (Table 1). Such multilevel sites are particularly useful for archaeomagnetic curve building when it was possible to establish a stratigraphy because this information can be included into the calibration curve modelling (Lanos 2004). Here the stratigraphic order can help to balance large dating errors, which are often much more important than those of directional information (Tarling & Dobson 1995). An outstanding example for helpfulness of such a stratigraphy modelling is the bread oven floor-sequence of Lübeck, where a full vector archaeomagnetic calibration curve could be obtained from 25 distinct layers for a time interval of about 450 yr (Schnepp *et al.* 2003, 2009). Existing stratigraphic information for all sites can be found in the supplementary material (Table S1, SupplementaryMaterialsA), that has been uploaded in the HISTMAG database (Arneitz *et al.* 2017b) and will be available online after publication. Stratigraphy of the new or updated sites is also shown in Fig. 2. Some important multilevel sites are described more detailed below.

The complexity of multilevel sites, as seen from site names and structure names in Table 1, led to the introduction of a sequence number. This newly introduced sequence number (Table S1, SupplementaryMaterialsA) consists of the two-digit ISO country code, three digits for the site and two digits for the feature(s), separated by underscores. The sequence number will be used for the HISTMAG database (Arneitz *et al.* 2017b) as unique site identifier, which is not necessarily given by the column 'name' of Table 1 or Table S1 (SupplementaryMaterialsA). A certain sequence

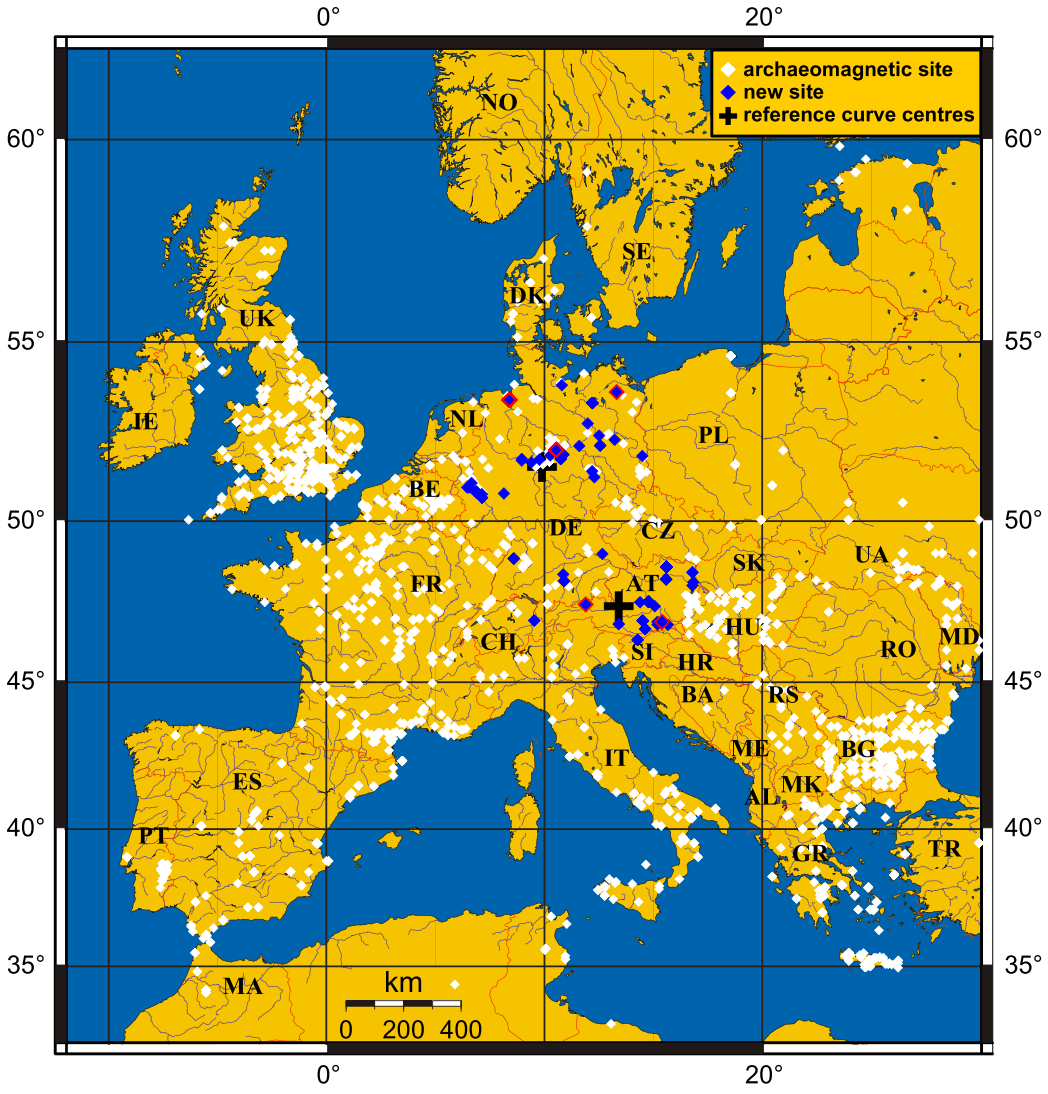

Figure 1. Map (Mercator projection) showing locations of archaeomagnetic sites in Europe taken from the HISTMAG database (white diamonds; Arneitz *et al.* 2017b). The newly investigated Austrian, German and Swiss sites are shown in blue. Black crosses are reference centres Göttingen and Radstadt. Five sites marked in red give unusual directions.

number (e.g. AT_003_04, Table S1, SupplementaryMaterialsA) may combine the results of several features when their age was not different, and directions agreed well. In these cases, a site mean was calculated from all results. Nevertheless, about a quarter of the sites provided two or three directions with different ages or with stratigraphic information. Nine sites are outstanding because they gave four or even many more directions, often together with a stratigraphy.

2.1.1 Meyenburg (Late Medieval/Modern Age)

The castle Meyenburg (Brandenburg, Germany) was mentioned for the first time in 1285 AD and was extensively investigated and renovated until 2002 (Goralczyk 2006; Müller & Patzschke 2006). During this renovation three hypocaustic heatings with stratigraphic relation could be sampled in the cellar as well as the walls of two ingles from the younger part of the building. All these features were made of brick and provided five archaeomagnetic directions (see Table S1, SupplementaryMaterialsA: no. DE_116_01– DE_116_05).

2.1.2 Thunau am Kamp (Early Medieval Age)

The early medieval settlement of Thunau am Kamp (Niederösterreich, Austria) consisted of a hill and a valley part (e.g. Szameit 2015). The valley part provided opportunities for extensive archaeomagnetic sampling in a time period that is sparsely represented in databases of central Europe. Here many pit houses had been excavated, each supplied with one or more ovens or fireplaces. Sometimes the superposition of the houses, their floor layers or their ovens provided direct stratigraphic information. Twenty-six features could be sampled and investigated and 25 mainly well constrained archaeomagnetic directions were obtained (Schnepp *et al.* 2015; Schnepp 2018; Table S1, SupplementaryMaterialsA: no. AT_010_01–AT_010_26).

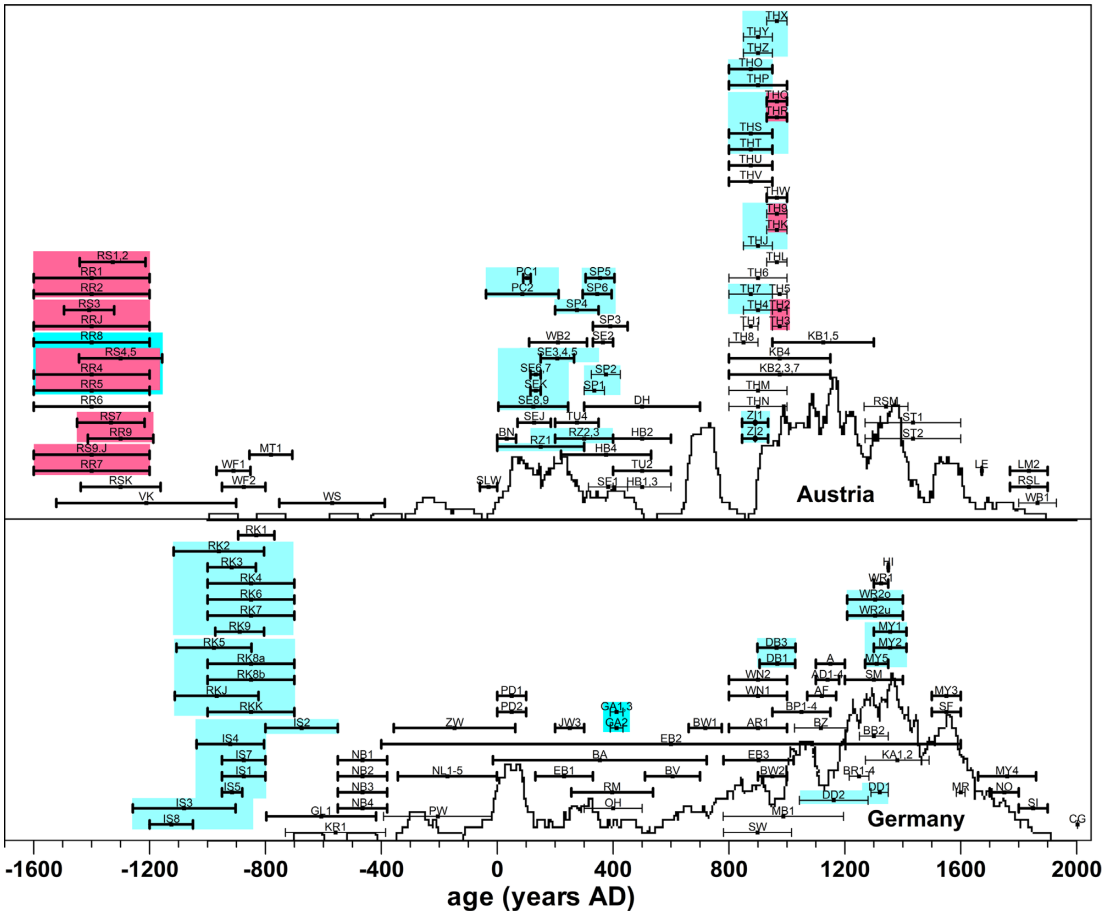

Figure 2. Cumulative temporal distributions of the published Austrian and German archaeomagnetic secular variation calibration curves (Schnepp & Lanos 2005, 2006) in comparison with age intervals of newly investigated Austrian, German and Swiss (♦) sites. Light lines indicate revised data (Table 3). Four German features are not shown because of the large dating intervals (GL2, LC) or their high age (LS, PA, *cf.* Table 1). Stratigraphic constraints are shown by pink boxes for contemporaneity, while blue shades indicate sequences from older (bottom) to younger (top) age.

2.1.3 St. Pölten (Roman Age)

The Roman town 'municipium aelium cetium' was founded in 121/22 AD and destroyed twice in 170 and 270 AD (Risy & Scherrer 2005). This settlement existed until 450 AD and is overbuilt by the modern town of St Pölten (Niederösterreich, Austria). The area excavated in the garden of the Diözesanmuseum comprised several buildings of which six structures were sampled in 2004. The sampled features belong to the last period and comprise hypocausts, fireplaces and a praefurnium. They were built with bricks, local rocks or baked clay and provided stratigraphic information (see Table S1, SupplementaryMaterialsA: no. AT_006_01–AT_006_06).

2.1.4 Semlach (Roman Age)

The location Semlach Eisner (Carinthia, Austria) was a centre of Noric iron production in Roman times and perhaps already earlier. Since 2003 the site was under interdisciplinary investigations including geophysical prospection and archaeological excavations (Cech 2014). Archaeological features of the smelting place comprise iron smelting furnaces, smithing and roasting hearths, lime pits, post holes, buildings and walls. Twelve of the iron smelting features have been investigated palaeomagnetically. The smelting activity lasted for a long time and can be divided roughly into at least three phases which are separated by levelling layers on which Roman buildings were found. Some of the furnaces showed several phases of use but they could not be sampled in detail. The site is dated by ceramics, coins and a fibula; two of the furnaces were dated by dendrochronology and one by an AMS radiocarbon age. Results of structures with similar ages have been combined, leading to a total of seven stratigraphically constrained directions (see Table S1, SupplementaryMaterialsA: no. AT_003_01–AT_003_07; Schnepp 2017).

2.1.5 Neuenbürg (Early Iron Age)

In Germany the oldest iron smelting furnaces are dated to the 6th century BC of the late Hallstatt period. The location Neuenbürg Grösseltal (Baden-Württemberg, Germany) was occupied for iron production in the late Hallstatt and early LaTène period (Gassmann *et al.* 2011; Gassmann & Schäfer 2014). The smelting took place in small (approximately 1 m diameter) domed furnaces with an integrated pit in front. An archaeological excavation unearthed six of them. In some cases, parts of the dome were still existent. Four

Table 1. New archaeomagnetic data: Sequence number (AT: Austria, CH: Switzerland, DE: Germany) provides a unique site identifier; site name (superscript: reference, see below); feature name; age as calendar date with a 99 per cent confidence interval and method of dating [archaeological estimate (arch.), calibrated radiocarbon age obtained from acceleration mass spectrometry (AMS) or beta counting (cC14), dendrochronological dating (DC), optically stimulated luminescence (OSL)]; number of independently oriented samples; declination; inclination (∗: direction unreliable; see text or Table S1, SupplementaryMaterialsA); precision parameter; 95 per cent confidence limit of characteristic remanent magnetisation (ChRM). References (1: Schnepp 2017; 2: Aidona *et al.* 2006; 3: Trapanese *et al.* 2008; 4: Schnepp 2011b; 5: Schnepp *et al.* 2015; 6: Schnepp 2018; 7: Schnepp 2008b; 8: Klemm *et al.* 2017; 9: Schnepp 2008b; 10: Schnepp 2010a; 11: Schnepp 2011a; 12: Schnepp 2015; 132: Schnepp 2016; 14: Schnepp & Brüggler 2016).

Sequence number	Site	Structure name	Age (yr A.D.)	Method	N	D (°)	I (°)	k	α_{95} (°)
AT_003_02	Semlach[1]	SE2	330–400	arch.	11	6.3∗	59.8∗	30	8.4
AT_003_03	Semlach[1]	SE3–5	150–265	arch.	26	357.8	62.1	105	2.8
AT_003_04	Semlach[1]	SE6,7	115–150	arch.	32	357.9	64.1	107	2.5
AT_003_05	Semlach[1]	SEK	115–150	arch.	9	352.8	58.5	163	4.0
AT_003_06	Semlach[1]	SE8,9	4–245	AMS	16	358.0	65.4	285	2.2
AT_003_07	Semlach[1]	SEJ	70–185	arch.	5	357.9∗	55.1∗	236	5.0
AT_004_02	Hemmaberg	HB2	400–600	arch.	11	–1.7	61.0	203	3.2
AT_004_03	Hemmaberg	HB4	220–531	AMS	7	10.2	67.5	194	4.3
AT_006_01	St.Pölten	SP3	330–450	arch.	14	6.1	61.9	76	4.4
AT_006_04	St.Pölten	SP5	300–400	arch.	12	353.9	56.4	185	3.4
AT_006_05	St.Pölten	SP6	300–400	arch.	8	351.3	62.3	370	2.9
AT_006_06	St.Pölten	SP4	200–350	arch.	8	354.0	62.2	145	4.0
AT_008_02	Eisenerz/Ramsau-S1	RS1,2	–1441 – –1214	AMS	27	0.1	67.8	214	1.9
AT_008_03	Eisenerz/Ramsau-S1	RR1	–1600 – –1200	arch.	7	0.8	64.0	220	4.1
AT_008_04	Eisenerz/Ramsau-S1[3]	RR2	–1600 – –1200	arch.	5	5.7	70.6	662	3.0
AT_008_05	Eisenerz/Ramsau-S1[2]	RS3	–1495 – –1322	cC14, AMS	10	1.6	67.7	232	3.2
AT_008_06	Eisenerz/Ramsau-S1	RRJ	–1600 – –1200	arch.	5	–13.3	67.6	75	8.9
AT_008_07	Eisenerz/Ramsau-S1[2]	RR8	–1600 – –1200	arch.	5	10.2	70.0	656	3.0
AT_008_08	Eisenerz/Ramsau-S1	RS4,5	–1418 – –1131	AMS	23	5.7	67.7	129	2.7
AT_008_09	Eisenerz/Ramsau-S1	RR4	–1600 – –1200	arch.	5	7.7	65.2	610	3.1
AT_008_10	Eisenerz/Ramsau-S1[2]	RR5	–1600 – –1200	arch.	6	4.1	68.9	212	4.6
AT_008_11	Eisenerz/Ramsau-S1	RR6	–1600 – –1200	arch.	9	3.5	67.3	116	4.8
AT_008_12	Eisenerz/Ramsau-S1[2]	RS7	–1450 – –1217	AMS	6	3.1	69.2	208	4.7
AT_008_13	Eisenerz/Ramsau-S1[3]	RR9	–1493 – –1267	AMS	11	4.6	62.7	370	2.4
AT_008_14	Eisenerz/Ramsau-S1	RS9,J	–1600 – –1200	arch.	28	2.8	69.2	246	1.7
AT_008_15	Eisenerz/Ramsau-S1	RR7	–1600 – –1200	arch.	12	2.1	65.1	206	3.0
AT_008_16	Eisenerz/Ramsau-S1	RSK	–1403 – –1127	AMS	8	358.6	69.4	182	4.1
AT_009_01	Karnburg[4]	KB1,5	950–1300	arch.	18	22.1	59.8	61	4.5
AT_009_02	Karnburg[4]	KB4	800–1150	arch.	9	21.0	63.7	92	5.4
AT_009_03	Karnburg[4]	KB2,3,7	800–1150	arch.	34	15.4	66.9	192	1.8
AT_010_01	Thunau[5]	TH1	850–900	arch.	16	13.4	69.1	315	2.1
AT_010_02	Thunau[5]	TH2	950–1000	arch.	16	14.3	71.1	681	1.4
AT_010_03	Thunau[5]	TH3	950–1000	arch.	14	8.5	71.2	406	2.0
AT_010_04	Thunau[5]	TH4	850–950	arch.	13	15.8	69.1	258	1.9
AT_010_05	Thunau[5]	TH5	950–1000	arch.	15	16.5	71.0	203	2.7
AT_010_06	Thunau[5]	TH6	800–1000	arch.	13	16.3	70.8	160	3.3
AT_010_07	Thunau[5]	TH7	800–950	arch.	17	6.3	69.8	344	2.6
AT_010_08	Thunau[5]	TH8	800–900	arch.	9	–2.7	70.0	689	2.0
AT_010_09	Thunau[5]	TH9	930–1000	arch.	14	17.5	67.4	139	3.4
AT_010_10	Thunau[5]	THK	930–1000	arch.	4	21.0	70.8	336	5.0
AT_010_11	Thunau[5]	THJ	850–950	arch.	12	18.4	71.5	183	3.2
AT_010_12	Thunau[5]	THL	930–1000	arch.	14	11.3	67.7	384	2.0
AT_010_13	Thunau[5]	THM	800–1000	arch.	13	0.3∗	61.3∗	194	3.0
AT_010_14	Thunau[5]	THN	800–1000	arch.	10	9.7	67.4	67	5.9
AT_010_15	Thunau[6]	THO	800–950	arch.	15	11.7	69.4	302	2.2
AT_010_16	Thunau[6]	THP	800–1000	arch.	15	15.5	73.2	466	1.8
AT_010_17	Thunau[6]	THQ	930–1000	arch.	15	15.2	71.3	530	1.7
AT_010_18	Thunau[6]	THR	930–1000	arch.	15	17.9	70.9	431	1.8
AT_010_19	Thunau	THS	800–950	arch.	15	15.4	72.4	703	1.4
AT_010_20	Thunau[6]	THT	800–950	arch.	28	9.8	71.6	617	1.6
AT_010_21	Thunau[6]	THU	800–950	arch.	15	12.5	70.3	228	2.5
AT_010_22	Thunau[6]	THV	800–950	arch.	13	9.0	71.4	603	1.7
AT_010_23	Thunau[6]	THW	930–1000	arch.	13	13.5	71.3	505	1.8
AT_010_24	Thunau	THX	930–1000	arch.	13	15.8	70.1	396	2.1
AT_010_25	Thunau	THY	850–950	arch.	10	8.8	69.6	516	2.1
AT_010_26	Thunau	THZ	850–950	arch.	13	10.4	69.2	90	4.4
AT_011_01	Trieben/versunkene Kirche	VK	–1522 – –901	cC14	10	348.9	65.8	39	7.9
AT_012_01	Teurnia	TU2	400–600	arch.	5	4.4	52.4	252	5.0

Table 1. Continued

Sequence number	Site	Structure name	Age (yr A.D.)	Method	N	D (°)	I (°)	k	α_{95} (°)
AT_012_02	Teurnia	TU4	200–350	arch.	11	353.6	54.8	275	2.8
AT_013_01	Bruckneudorf	BN	0–65	arch.	12	–11.1∗	79.2∗	145	3.6
AT_014_02	Wörterberg	WB2	100–300	arch.	24	–4.5	61.9	270	1.8
AT_015_01	Petronell-Carnuntum	PC1	90–116	arch.	19	358.0	64.7	171	2.6
AT_015_02	Petronell-Carnuntum	PC2	–39–212	AMS	9	22.8	68.7	58	6.8
AT_016_01	Stainz	SLW	–60–0	arch.	31	–13.1∗	63.0∗	9	9.2
AT_017_01	Leoben	LE	1672–1673	hist.	8	12.4∗	56.5∗	38	9.1
AT_018_01	Deutschlandsberg	DH	300–700	arch.	23	5.5	56.8	95	3.1
AT_019_01	Rannersdorf	RN	–4750 – –4250	arch.	15	–6.2	61.8	396	1.9
AT_020_01	Retznei	RZ2,3	200–400	arch.	31	–4.4	58.9	175	2.0
AT_020_02	Retznei	RZ1	0–300	arch.	19	–2.6	63.9	270	2.0
AT_021_01	Wettmannstätten	WS	–752 – –388	AMS	18	17.9	71.8	566	1.5
AT_022_01	Weitendorf/Faltikögerl	WF1	–969 – –852	AMS	29	31.8	69.3	98	2.7
AT_022_02	Weitendorf/Faltikögerl	WF2	–950 – –800	arch.	21	18.7	71.0	58	4.2
AT_023_01	Maukental	MT1	–855 – –707	DC	21	41.6	72.7	87	3.4
AT_026_01	Eisenerzer Ramsau[8]	LM2	1770–1900	arch.	4	–2.3	64.3	131	8.1
CH_017_01	Zizers	ZI1	850–940	arch.	26	17.1	67.0	205	2.0
CH_017_02	Zizers	ZI2	850–940	arch.	19	16.4	63.4	162	2.6
DE_053_02	Pestenacker	PA	–3495 – –3480	DC	19	354.3	58.6	45	5.1
DE_100_02	Jänschwalde/Tagebau[9]	JW3	200–300	arch.	22	2.5	63.7	93	3.2
DE_101_01	Altenbeken/Dübelsnacken[10]	AD1–4	1100–1180	arch.	8	20.2	62.8	361	2.9
DE_102_01	Altenbeken/Füllenberg[10]	AF	1070–1170	arch.	20	19.9	67.3	103	3.2
DE_103_01	Brühl/Schloss Augustus-burg[11]	BA	–15–723	OSL	31	–4.9	66.6	352	1.4
DE_104_01	Rommerskirchen[11]	RM	256–538	AMS	24	0.5	65.1	400	1.5
DE_105_01	Bonn/Bechlinghoven[11]	BV	510–700	arch.	17	358.3	71.9	167	2.8
DE_106_01	Bornheim/Walberberg[11]	BW1	661–775	AMS	28	9.0	74.1	230	1.8
DE_106_03	Bornheim/Walberberg[11]	BW2	900–1000	arch.	8	18.2	68.1	1253	1.6
DE_107_01	Derenburg	DB3	898–1030	AMS	12	15.7	70.0	224	2.9
DE_107_02	Derenburg[11]	DB1	895–1018	AMS	21	20.2	70.7	206	2.2
DE_108_01	Spielberg[12]	SI	1800–1900	arch.	16	345.9	64.8	699	1.4
DE_109_01	Schindlfurth[12]	SF	1500–1600	arch.	21	346.9∗	60.8∗	73	3.8
DE_110_01	Elbingerode[13]	EB1	132–330	AMS	26	4.1	67.8	351	1.5
DE_110_02	Elbingerode[13]	EB2	–400–1600	arch.	14	16.6	68.7	210	2.7
DE_110_03	Elbingerode[13]	EB3	781–1023	AMS	11	13.2	73.8	147	3.8
DE_113_01	Goch/Asperden[14]	GA1,3	390–434	arch.	20	354.5	65.5	255	2.0
DE_113_02	Goch/Asperden[14]	GA2	390–434	arch.	14	5.2∗	60.8∗	264	2.5
DE_114_01	Klein-Neuleben	NL1–5	–343 – –1	AMS	28	355.7	68.6	73	3.2
DE_115_01	Zwenkau	ZW	–357–62	AMS	14	0.5	68.0	229	2.6
DE_116_01	Meyenburg	MY1	1300–1413	arch.	22	4.1	57.8	222	2.2
DE_116_02	Meyenburg	MY2	1300–1413	arch.	10	5.6	58.4	252	3.1
DE_116_03	Meyenburg	MY5	1270–1350	arch.	14	10.0	60.3	157	3.2
DE_116_04	Meyenburg	MY3	1500–1600	arch.	14	12.0	67.6	303	2.3
DE_116_05	Meyenburg	MY4	1660–1860	arch.	16	349.5	73.1	354	2.0
DE_117_01	Leipzig/Schkreuditz	LS	–2861 – –2466	AMS	32	3.7	69.8	185	1.9
DE_118_01	Altenzaun/Rosenhof	AR1	800–1000	arch.	25	20.4	75.7	129	2.6
DE_119_01	Pingsdorf	BP1–4	950–1150	arch.	53	16.7	67.4	345	1.4
DE_120_01	Schmessen	SM	1200–1400	arch.	14	6.0	53.6	124	3.6
DE_121_01	Neuenbürg	NB1	–550 – –380	arch.	15	325.2	73.3	54	5.2
DE_121_02	Neuenbürg	NB2	–550 – –380	arch.	10	341.3	61.3	90	5.1
DE_121_03	Neuenbürg	NB3	–550 – –380	arch.	14	350.8	75.6	38	6.6
DE_121_04	Neuenbürg	NB4	–550 – –380	arch.	20	349.8	69.1	146	2.7
DE_122_01	Paffendorf	PD1	0–100	arch.	19	354.1	67.2	123	3.0
DE_122_02	Paffendorf	PD2	0–100	arch.	9	1.0	62.9	148	4.2
DE_123_01	Lich/Steinstraß	LC	–2200–0	arch.	14	5.7	62.0	120	3.6
DE_124_01	Wachtberg/Nieder-bachem	WN2	800–1000	arch.	16	14.8	67.0	341	2.0
DE_124_02	Wachtberg/Nieder-bachem	WN1	800–1000	arch.	17	6.0	69.9	335	2.0
DE_125_01	Hildesheim/Dom	HI	1349–1351	hist.	24	6.6	57.4	60	3.8
DE_126_01	Nochten	NO	1700–1800	arch.	21	339.4	68.5	447	1.5
DE_127_01	Walkenried/Kloster	WR1	1300–1350	arch.	11	7.9	55.7	98	4.6
DE_127_03	Walkenried/Kloster	WR2o	1208–1400	arch.	12	7.9	56.6	210	3.0
DE_127_04	Walkenried/Kloster	WR2u	1208–1400	arch.	13	18.1	62.1	171	3.2
DE_128_01	Glocksin	GL1	–797 – –418	AMS	7	69.8	74.8	151	4.9
DE_128_03	Glocksin	GL2	–3500 – –600	arch.	9	–5.7	65.0	107	5.0
DE_129_01	Rodenkirchen/Hahnen-knooper-Mühle (HK-M)	RK1	–894 – –769	AMS	9	59.0	71.8	181	3.8

Table 1. Continued

Sequence number	Site	Structure name	Age (yr A.D.)	Method	N	D (°)	I (°)	k	α_{95} (°)
DE_129_02	Rodenkirchen/(HK-M)	RK2	–1117 – –805	AMS	9	43.2	66.8	192	3.7
DE_129_03	Rodenkirchen/(HK-M)	RK3	–1000 – –833	AMS	12	15.2	69.2	235	2.8
DE_129_04	Rodenkirchen/(HK-M)	RK4	–1000 – –700	arch.	9	53.7	73.9	201	3.6
DE_129_05	Rodenkirchen/(HK-M)	RK6	–1000 – –700	arch.	13	36.4	69.7	643	1.6
DE_129_06	Rodenkirchen/(HK-M)	RK7	–1000 – –700	arch.	9	39.0	73.6	134	4.5
DE_129_07	Rodenkirchen/(HK-M)	RK9	–973 – –805	AMS	8	41.2	71.7	279	3.3
DE_129_08	Rodenkirchen/(HK-M)	RK5	–1107 – –848	AMS	10	62.1	68.9	116	4.5
DE_129_09	Rodenkirchen/(HK-M)	RK8a	–1000 – –700	arch.	12	35.4	72.5	200	3.1
DE_129_10	Rodenkirchen/(HK-M)	RK8b	–1000 – –700	arch.	15	53.1	73.6	201	2.7
DE_129_11	Rodenkirchen/(HK-M)	RKJ	–1113 – –824	AMS	9	41.4	74.9	443	2.5
DE_129_12	Rodenkirchen/(HK-M)	RKK	–1000 – –700	arch.	10	42.0	74.4	159	3.8
DE_130_01	Isingerode/Isiburg	IS2	–800 – –550	arch.	18	30.5	68.4	127	3.1
DE_130_02	Isingerode/Isiburg	IS4	–1038 – –805	AMS	10	5.9	67.3	257	3.0
DE_130_03	Isingerode/Isiburg	IS7	–950 – –800	arch.	8	33.3	70.4	133	4.8
DE_130_04	Isingerode/Isiburg	IS1	–950 – –800	arch.	12	26.5	66.8	100	4.4
DE_130_05	Isingerode/Isiburg	IS5	–950 – –880	arch.	13	41.6	66.6	45	6.2
DE_130_06	Isingerode/Isiburg	IS3	–1258 – –903	AMS	15	27.7	68.0	53	5.3
DE_130_07	Isingerode/Isiburg	IS8	–1200 – –1050	arch.	7	39.2	64.5	69	6.5
DE_132_01	Augsburg	A	1100–1200	arch.	2	19.6∗	60.4∗	1369	6.8

of these furnaces dated to the 4th century BC were sampled (see Table S1, SupplementaryMaterialsA: no. DE_121_01–DE_121_04). Unfortunately, the archaeological situation did not provide a stratigraphic order.

2.1.6 Rodenkirchen (Late Bronze Age/Early Iron Age)

The oldest settlement known so far in the marsh in Northern Germany is located close to the Weser estuary at the border of the village Rodenkirchen (Niedersachsen, Germany). During Late Bronze age countrymen erected at least three houses, one as a farmstead-barn-combination with three naves (Strahl 2004). This house was excavated completely between 1996 and 2001 and about 2000 posts have been found. Three phases of occupation of the place and two renovations of the house can be seen. Numerous conventional radiocarbon datings performed on many of the posts used for the house and on the surrounding fences and other wooden objects gave mainly ages (1σ standard deviation) falling in the 10th and 9th centuries BC but do not allow to distinguish the occupation phases. Among the finds are remains of bronze working (Strahl 2005). According to Strahl (2007) a precise archaeological dating based on pottery is difficult and comprises the periods IV to VI of the Nordic Bronze age (after Montelius) which can be attributed to the time interval from 1125 to 575 BC (Lanting & Plicht 2003). The bulk of the pottery is related to the transition Late Bronze to Early Pre-Roman Iron Age (period V to VI) which dates around 750 BC according to Lanting & Plicht (2003) and seems to be related with the abandonment of the house, while the radiocarbon ages seem to be related with its construction (Strahl 2007). A restriction in age is given because the plateaus on which the archaeological structures were found are underlain by sediments of the Dunkirk transgression Ia. This gives a *terminus post quem* in the time range of 1000 to 800 BC for the settlement activity and the existence of the house attributed to phase II lasted presumably less than a century (Strahl 2007). Inside the house two piles consisting of several hearths or oven floors have been found, while outside two working platforms with fireplaces existed which are attributed to phase III. In this last phase the piles in the abandoned house were still in use as fireplaces. Palaeomagnetic sampling comprised 12 hearths and fireplaces (see Table S1, SupplementaryMaterialsA: DE_129_01–DE_129_12) which can be associated with phases II and III of the house and they provide a stratigraphy as seen, for example in Fig. 3.

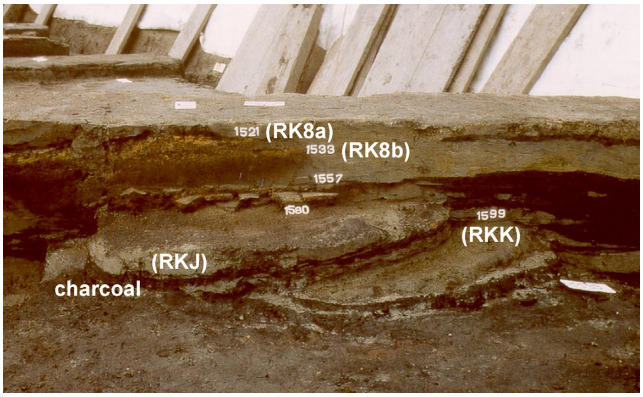

Figure 3. Photograph of the pile of central hearth plates found in the Bronze Age house of Rodenkirchen (RK). The names of the sampled plates are given in brackets (*cf.* Table 1).

2.1.7 Isingerode (Late Bronze Age/Early Iron Age)

Close to Isingerode (Niedersachsen, Germany) a Bronze Age castle existed from about 1300 BC to the beginning of the Iron Age. Its dimension can be deduced from areal images which show a hillfort with a diameter of about 150 m (Steinmetz 2008). Six burnt horizons giving evidence for several attacks or destructions of the castle were identified during the excavations of the rampart which started in 1998. Between 2007 and 2014 eight of the features, burnt layers and fireplaces, were sampled and seven were investigated successfully (see Table S1, SupplementaryMaterialsA: DE_130_01–DE_130_07). The sampled features are related to the stratigraphy of the site and represent three phases of occupation of the castle in the Late Bronze and Early Iron age.

2.1.8 Eisenerz/Ramsau-S1 (Middle Bronze Age)

'S1' is a prehistoric copper smelting site in the Ramsau valley of Eisenerz (Styria, Austria; Klemm 2003, 2004, 2006). It was excavated in several campaigns between 1992 and 2006. A large number of Eisenerz S1 archaeological features were identified, comprising 11 smelting furnaces, 10 roasting hearths, many pits of varying size and uses, and 3 slag heaps, all of Middle to Late Bronze age. Additionally, a large charcoal pit was found which is dated to the Late Medieval period. The copper smelting was performed in twin furnaces, arranged side by side, and accompanied by a roasting hearth. The walls of the furnaces as well as the rims of the roasting hearths were built using local rocks. In the Western part of the site for three of the twin furnaces the chronological record is well documented by stratigraphy given by association of furnaces and roasting hearths and superposition of some of them. For the rest of the place stratigraphy is less clear as it is considerably disturbed by the Medieval charcoal pit. A final stratigraphic correlation is not yet available. Structures sampled for the palaeomagnetic investigation were the charcoal pit (Klemm *et al.* 2005), nine roasting hearths and nine furnaces (see Table S1, SupplementaryMaterialsA: AT_005_01, AT_005_02–AT_005_16, respectively).

Preliminary results from this site have been published (Klemm *et al.* 2005; Aidona *et al.* 2006; Trapanese *et al.* 2008) and here the results are completed, updated or refined and split into 14 archaeodirections associated with individual structures. Accordingly, the data of Aidona *et al.* (2006) have to be flagged as double in existing archaeomagnetic databases.

3 DATING OF CHARCOAL OR WOOD AND RESULTS

Age dating of the new sites was mainly provided by the archaeologists using finds, stratigraphic relations or historical documents. Additionally, for about 30 per cent of the features conventional or accelerator mass spectrometry (AMS) radiocarbon dating or sometimes dendrochronological dating of charcoal or wood was used when such data were available. Table 2 lists results of radiocarbon dating, of which 17 were provided by the archaeologists. All conventional radiocarbon ages were calibrated using the 2009 calibration curve (Reimer *et al.* 2009) and the 99 per cent probability interval was calculated. Even if it was not continuous the lowest and highest age values are given in Table 2 (Tables 1 and S1, SupplementaryMaterialsA) as age interval. One date was rejected because it was modern but the archaeomagnetic direction was not (*cf.* Tables 2 and 1, AT_022_01:WF1).

Most of radiocarbon dating was performed for features dating before Christ in order to support the archaeological dating. Eight charcoal samples related to the sampled structures of Rodenkirchen have been dated with the AMS technique (Table 2). They are in good agreement with conventional ^{14}C datings (Strahl 2005; Strahl 2007) performed on the wood samples. However, two samples taken from the neighbouring occupation layers have been rejected because considerably older ages were obtained (Table 2: RK4, RK6), presumably due to old wood effects. Generally assigning the age for the two phases of occupation was difficult because of the high dispersion of the radiocarbon data and presumed old wood effects, but there is little evidence that the place was still in use during the Hallstatt radiocarbon plateau which started around 700 BC. Finally, relatively wide age ranges have been assigned lasting from 750 to 600 BC for phase III and 1000–700 BC for phase II although the phases must have been considerably shorter. This will allow the Bayesian curve estimation to find the posterior age intervals by the synopsis of all data.

Three charcoal samples were taken from the layers at Isingerode (IS) and were dated with the AMS technique in Erlangen (Germany). While two of them are in good agreement with the archaeological age determined on potsherds and other finds another (IS1 see Table 2) was considerably older. As it was taken from a plank presumably used for stabilization of a wall the old wood effect prevented further use for dating of the burnt layer.

Further three sites are dated to the transition from late Bronze age to early Iron Age (GL1, WF1, WS), while two other sites (VK, Eisenerz-S1) belong to the Bronze Age. Dating of the structures of S1 (Eisenerz, RS RR) is based on archaeological finds, as well as dating of charcoals with the radiocarbon method (see Tables 2 and S1, SupplementaryMaterialsA). Apart from the re-use in medieval times the prehistoric use shows a stratigraphy for the Middle Bronze Age and the ages range from the 16th to the 13th century BC (Klemm 2006). Two conventional radiocarbon ages were published by Klemm (2003, 2004) and six AMS measurements were performed at VERA (Vienna Environmental Research Accelerator) in Austria.

The oldest radiocarbon date was obtained at the end of the Neolithic (LS see Table 2). Furthermore, 10 age entries have been updated with new age information (Table 3), two of them by using dendrochronological ages.

4 LABORATORY PROCEDURES AND ANALYSIS

Treatment of the samples was mainly carried out in the palaeomagnetic laboratory Gams of the University of Leoben (Austria), as well as in the palaeomagnetic laboratory Grubenhagen of the LIAG (Germany) or at the Conrad Observatory (ZAMG, Austria). Some rockmagnetic experiments were carried out at GFZ (Potsdam).

4.1 Sample consolidation and cutting

The brittle block samples and soft cores, sometimes also brittle rock material, were consolidated with *Wacker Stone Strengthener OH* (Wacker Chemie, Vienna) following Schnepp *et al.* (2008). Block samples were then cut into cubes (25 mm, 20 mm, or 14 mm side length) while soft cores or drill cores were separated into cylinders (22 mm length). Samples taken with the English technique (Clark *et al.* 1988) were either trimmed to fit them into plastic boxes (20 mm) without removing the acryl glass, or, if the sample was big enough, cut into cubes by removing the orientation plate. Samples in plastic containers could be measured without preparation.

4.2 Measurements

The natural remanent magnetization (NRM) was measured mainly with cryogenic magnetometers, bulk susceptibility with a Minikappa bridge (AGICO) and also mass was determined. For 19 sites Thellier viscosity tests (Thellier & Thellier 1944) have been performed. In some cases, specimens have been preferred which, taking into account their NRM directions, presumably did not carry any secondary components. Thermomagnetic curves were determined in air using a KLY3 Agico susceptibility meter with fitted furnace up to 650° C. In the palaeomagnetic laboratory of the GFZ Potsdam, acquisition and back field curves of isothermal remanent magnetization (IRM) were carried out with a Princeton Micromag

Table 2. List of archaeological features with results of radiocarbon dating obtained from acceleration mass spectrometry (AMS) or beta counting (conv.) together with archaeological age estimate according to reference or personal communication during fieldwork; 1: taken from reference, 2: not used, modern charcoal, 3: provided by C. Gutjahr, 4: provided by F. Verse, 5: revised dating, provided by R. Kuhn, 6: provided by M. Müssemeier, 7: provided by G. Alper, 8: ERL-14 041 not used, see reference, 9: provided by J. Brandt, 10: not used, old wood). The first column is referring to Table 1. All ages have been calculated with OxCal (Bronk Ramsey 2009) using the 2009 version of the calibration curve (IntCal09: Reimer *et al.* 2009 on 99 per cent probability (2.58σ).

Sequence number	Site/structure name	Archaeological age estimate (centuries)	Reference	^{14}C method	^{14}C-age (a BP)	$\pm 1\sigma$ (a)	Age ($\pm 2.58\sigma$) (cal. AD)	Median Age (cal. AD)	Laboratory number	delta^{13}C (‰)
AT_003_06	Semlach SE89	end of 1st to beginning of 2nd AD	Schnepp 2017	AMS	1884	41	4–245	124.5	ERL-12 850	–24.0
AT_004_03	Hemmaberg HB4	5th AD	Glaser 1991	AMS	1697	41	220–531	375.5	ERL-12 848	–26.0
AT_005_01	Eisenerz Ramsau-S1 RSM	13th to 1st half 15th AD	Klemm *et al.* 2005	conv.[1]	640	50	1266–1418	1342.0	Beta-99 260	not reported
AT_007_01	Eisenerz Ramsau RSL	1770 to 1900 AD	Klemm *et al.* 2005	conv.[1,2]	100	60	1665–1955	1810.0	Beta-223 624	not reported
AT_008_02	Eisenerz Ramsau-S1 RS1,2	16th to 13th BC	Klemm 2003	AMS	3080	35	–1441 – –1214	–1327.5	VERA-3488	–23.7 ± 0.7
AT_008_05	RS3	16th to 13th BC	Klemm 2003	conv.[1]	3050	80			Beta 99 261	–26.3
AT_008_05				AMS	3165	35			VERA-3489	–22.7
AT_008_05			weighted	mean	3147	32	–1495 – –1322	–1408.5		
AT_008_08	RS4,5	16th to 13th BC	Klemm 2003	AMS	3045	35	–1418 – –1131	–1274.5	VERA-3858	–22.7 ± 0.4
AT_008_12	RS7	16th to 13th BC	Klemm 2003	AMS	3090	35	–1450 – –1217	–1333.5	VERA-3857	–25.7 ± 0.4
AT_008_13	RR9	16th to 13th BC	Klemm 2003	AMS	3115	35	–1493 – –1267	–1380.0	VERA-3859	–27.6 ± 0.6
AT_008_16	RSK	16th to 13th BC	Klemm 2003	AMS	3020	35	–1403 – –1127	–1265.0	VERA-3860	–23.9 ± 0.4
AT_011_01	Trieben, versunkene Kirche VK	16th to 13th BC	Klemm 2003	conv.[1]	3010	100	–1522 – –901	–1211.5	VRI 657	not reported
AT_015_02	Petronell-Carnuntum PC2	90 to 117 AD	Kandler 2008 (pers. communication)	AMS	1930	35	–39–212	86.5	VERA-3491	–28.0 ± 2.1
AT_021_01	Wettmannstätten WS	late Bronze to Early Iron Age	Fuchs 2010 (pers. communication)	AMS	2396	41	–752 – –388	–570.0	ERL-12 847	–25.4
AT_022_01	Weitendorf Faltikögerl WF1	Ha B	Gutjahr 2018	AMS[2]	53	41	1681–1955	1818.0	ERL-12 846	–27.8
AT_022_01				AMS[3]	2764	25			MAMS27887	–26.1 ± 2.0
AT_022_01				AMS[3]	2740	25			MAMS27888	–24.5 ± 2.0
AT_022_01				AMS[3]	2721	24			MAMS27889	–25.6 ± 2.0
AT_022_01				AMS[3]	2834	27			MAMS27890	–24.4 ± 2.0
AT_022_01				AMS[3]	2787	27			MAMS27891	–27.9 ± 2.0
AT_022_01				AMS[3]	2670	30			Beta-449 550	–26.1
AT_022_01			weighted	mean	2754	11	–969 – –852	–910.5		
DE_088_01	Haiger/Kalteiche KA1	late 14th to early 15th AD	Verse 2008	conv.[4]	550	25			KI-4958	–25.8
DE_088_01	Haiger/Kalteiche KA2	late 14th to early 15th AD	Verse 2008	conv.[4]	510	60			Beta-148 238	–25.0
DE_088_01	Haiger/Kalteiche KA12		weighted	mean	544	23	1271–1491	1381.0		
DE_098_01	Magdeburg MB1	10th AD	Schnepp & Lanos 2005; Kuhn *et al.* 2003	AMS[5]	1058	58	780–1195	987.5	Erl-7916	not reported
DE_104_01	Rommerskirchen RM	50 to 355 AD	Schnepp 2011a	AMS	1652	41	256–538	397.0	ERL-12 845	–26.0
DE_106_01	Bornheim Walberberg BW1	2nd half of 8th	Schnepp 2011a	AMS[6]	1290	23	661–775	718.0	KIA31226	–25.7 ± 0.2
DE_107_01	Derenburg DB3	10th AD	Schnepp 2011a	AMS[7]	1044	25	898–1030	964.0	KIA41794	–25.4 ± 0.2
DE_107_02	DB1	10th AD	Schnepp 2011a	AMS[7]	1090	36			KIA41793	–27.5 ± 0.1
DE_107_02				AMS[7]	1065	26			KIA41792	–27.5 ± 0.1
DE_107_02			weighted	mean	1074	21	895–1018	956.5		
DE_110_01	Elbingerode EB1	not estimable	Schnepp 2016	AMS[8]	1793	21	132–330	231.0	KIA-44 056	–24.7 ± 0.1
DE_110_03	Elbingerode EB3	not estimable	Schnepp 2016	AMS	1099	41	781–1023	902.0	Erl-14 042	–28.5
DE_114_01	Klein-Neuleben NL1–5	end of 2nd BC to first half of 1st AD	Brandt 2003 (pers. communication)	AMS[9]	2094	25	–343 – –1	–172.0	KIA19872	not reported
DE_115_01	Zwenkau ZW	2nd half of 1st BC to 1st half of 1st AD	Kampen 2004 (pers. communication)	AMS	2085	45	–357-62	–147.5	ERL-14 038	–29.1
DE_117_01	Leipzig Schkreuditz LS	Funnelbeaker culture	Friederich 2005 (pers. communication)	AMS	4045	35	–2861 – –2466	–2663.5	VERA-3490	–26.0 ± 1.0
DE_128_01	Glocksin GL1	late Bronze to Early Iron Age	Neutzer 2003	AMS	2519	32	–797 – –418	–607.5	KIA12354	–24.2 ± 0.1
DE_129_01	Rodenkirchen/Hahnenknooper Mühle RK1	9th to 7th BC	Strahl 2005	AMS	2635	30	–894 – –769	–831.5	KIA10674	–28.1 ± 0.1
DE_129_02	RK2	9th to 7th BC	Strahl 2005	AMS	2837	28	–1117 – –805	–916.5	KIA15675	–27.8 ± 0.1
DE_129_03	RK3	9th to 7th BC	Strahl 2005	AMS	2769	24	–1000 – –833	–916.5	KIA15678	–26.9 ± 0.2
DE_129_04	RK4	9th to 7th BC	Strahl 2005	AMS[9]	2843	33	–1188 – –898	–1043.0	KIA12356	–27.1 ± 0.2
DE_129_05	RK6	9th to 7th BC	Strahl 2005	AMS[9]	2861	24	–1186 – –919	–1052.5	KIA15679	–25.0 ± 0.1
DE_129_07	RK9	9th to 7th BC	Strahl 2005	AMS	2729	30	–973 – –805	–889.0	KIA14405	–27.2 ± 0.1
DE_129_08	RK5	9th to 7th BC	Strahl 2005	AMS	2815	26	–1107 – –848	–977.5	KIA15676	–25.4 ± 0.1
DE_129_11	RKJ	9th to 7th BC	Strahl 2005	AMS	2795	42	–1113 – –824	–968.5	KIA14403	–24.9 ± 0.1
DE_130_04	Isingerode Isiburg IS1	Ha B2/3	Steinmetz 2008	AMS[10]	3072	41	–1448 – –1132	–1290.0	ERL-12 843	–24.4
DE_130_02	IS4	Ha B3	Steinmetz 2008	AMS	2756	43	–1038 – –805	–921.5	ERL-14 039	–24.8
DE_130_06	IS3	Ha A1–2	Steinmetz 2008	AMS	2874	45	–1258 – –903	–1080.5	ERL-14 040	–24.3

AGFM for small chips (some mg) and some thermomagnetic curves were determined using a variable field translation balance (VFTB).

Alternating field (AF) demagnetization was performed using a 2 G device (150 mT) in line with the magnetometer, while for thermal demagnetisation a MMTD20 or MMTD60 oven (Magnetic Measurements) was used. Rather strong (>5 Am^{-1}) or large (25 mm cubes) specimens were measured in the laboratory of the LIAG (Grubenhagen) using a 2 G cryogenic magnetometer with large

Table 3. Revised archaeomagnetic data: Same columns as in Table 1; additionally kind of structure; and laboratory treatment (AF: alternating field demagnetisation, Th: thermal demagnetisation, Tv: viscosity test, Te: ChRM obtained from Thellier experiments). All entries changed with respect to the reference are highlighted in bold. References (1: Schnepp & Lanos 2006; 2: Klemm *et al.* 2005; 3: Klemm *et al.* 2017; 4: Trapanese *et al.* 2008; 5: Krenn 2005; 6 Schnepp *et al.* 2004; 7: Biermann 2010; 8: Schnepp & Lanos 2005; 9: Verse 2008; 10: Schnepp *et al.* 2016).

Sequence number	Site	Structure name	Age (yr A.D.)	Method	N	D (°)	I (°)	k	α_{95} (°)	Kind of structure	Treatment
AT_002_01	Stillfried[1]	ST1	**1270**–1600	arch.	**8**	**13.3**	**74.0**	**566**	**2.3**	oven	AF,Th
AT_002_02	Stillfried[1]	ST2	**1270**–1600	arch.	**13**	**2.5**	**66.1**	**779**	**1.5**	oven	AF,Th, **Tv**
AT_003_01	Semlach[1]	SE1	**315–450**	**DC, arch.**	7	–3.0	53.5	152	4.9	iron-furnace	AF,Th, Tv
AT_004_01	Hemmaberg	**HB1,3**	**400–600**	arch.	**23**	**6.8**	**63.7**	**82**	**3.4**	**hypocaust, fireplace**	AF,Th
AT_005_01	Eisenerz/Ramsau-S1[1,2]	RSM	**1266–1418**	**cC14**	11	**4.7**	61.5	**380**	**2.3**	charcoal-pit	AF,Th,**Te**
AT_006_03	St.Pölten[1]	SP1	**300–370**	arch.	**11**	**–1.6**	**59.1**	**238**	3.0	hypocaust	AF,Th
AT_006_02	St.Pölten[1]	SP2	**325**–425	arch.	**18**	**–1.1**	**61.6**	**235**	**2.3**	hypocaust	AF,Th,**Te**
AT_007_01	Eisenerz/Ramsau[2,3]	RSL	**1770–1900**	arch.	**15**	**–7.4**	**59.0**	**149**	**3.1**	charcoal-pile	AF,Th
AT_014_01	Wörterberg[4,5]	WB1	**1800–1930**	**hist**.	**15**	**–3.3**	**57.0**	**527**	**1.7**	pottery-kiln	AF,Th,**Te**
DE_033_01	Belzig[6]	BZ	**1026**–1208	cC14	12	**10.6**	**63.3**	**278**	2.5	pottery-kiln	AF,Th,**Te**
DE_039_01	Schnapsweg[6]	SW	**781**–1016	cC14, AMS	12	**24.6**	**65.7**	**246**	2.8	smelting-furnace	AF,Th,**Te**
DE_042_01	**Damsdorf**[6,7]	DD1	**1290–1350**	arch.	**7**	**7.0**	**66.0**	**403**	**3.0**	lime-furnace	AF,Th
DE_042_02	**Damsdorf**[6,7]	DD2	**1043**–1280	**cC14**	9	**17.1**	**61.5**	**489**	**2.3**	bread-oven	AF,Th, **Tv,Te**
DE_043_01	Pinnow[6]	PW	**–392** – –18	cC14	18	**–25.0**	**69.6**	**190**	**2.5**	pottery-kiln	AF,Th,**Te**
DE_048_01	Ohrum[6]	OH	**300–500**	arch.	9	7.5	71.3	170	4.0	fire-place	AF,Th
DE_050_01	Krackow[6]	KR1	**–731** – –385	AMS	23	**14.5**	**72.3**	**410**	**1.5**	burnt pit	AF,Th,**Te**
DE_081_01	Rabental/Meiler[8]	MR	**1585–1615**	DC	15	4.1	69.8	88	1.9	charcoal-pile	AF,Th
DE_087_01	**Fredelsloh/Bengerode**[8]	BR1–4	**1215**–1283	AMS	**49**	**8.3**	**63.3**	**130**	**1.8**	pottery-kilns 1–4	AF,**Th**
DE_097_01	Brandenburg[8]	BB2	**1250**–1350	arch.	**22**	**14.1**	**61.4**	**117**	**2.9**	pottery-kiln	AF,**Th**
DE_088_01	Haiger/Kalteiche[8,9]	KA1,2	**1271–1491**	cC14	16	9.9	59.4	254	2.3	lime kilns	AF
DE_098_01	Magdeburg[8]	MB1	**780–1195**	**AMS**	**18**	**18.4**	**70.8**	**287**	**2.0**	hypocaust	AF,**Th**
DE_111_01	Coppengrave[10]	CG	**2003**–2003	hist.	20	**1.7**	**66.2**	**630**	**1.3**	pottery-kiln	AF,Th,**Te**

diameter (120 mm) and the external AF device MI AFD 300 (or AFD 200) as well as a MI TD 700 oven (all Magnon International). At ZAMG laboratory an Agico JR6 spinner magnetometer and ASC D-2000 alternating field demagnetizer or MMTDSC thermal demagnetizer (Magnetic Measurements) were used. In order to save untreated specimens for palaeointensity experiments for some structures, for which only a few samples had been taken, the viscosity corrected direction has been used instead of a characteristic remanence. AF demagnetizations were performed with 5–15 steps starting with 2, 3 or 5 mT. The steps were not equidistant and much wider for the higher fields. Demagnetization was continued normally to at least 100 mT, except when the magnetization had already been removed. When more than 10 per cent of the NRM was still left after the 100 mT step some higher steps up to 300 mT were also performed. For structures with only weak secondary components a detailed demagnetization was only done for a few specimens while most specimens were demagnetized with a smaller set of steps. Thermal demagnetizations started between 100 and 200 °C and were performed with a 50 °C increment up to 550 or 650 °C. In some cases, temperatures above 600 °C with steps of 625, 650 and 680 °C were used. The thermal demagnetization was stopped earlier, if the specimens showed an increase of magnetization due to thermal alteration (see below) after an initial continuous decrease of magnetization. Whenever possible, at least one AF and thermal demagnetization was performed on specimens of each sample (*cf.* Table S1, SupplementaryMaterialsA). In a few cases only thermal demagnetization was done, e.g. for reheated bricks (Table 1, e.g. AT_06_05). In other cases, thermal demagnetisation was sometimes avoided, for example when only a few, not well heated specimens were available (e.g. Table 1, e.g. AT_06_05).

5 RESULTS

5.1 Rock magnetic investigations

Measurements of bulk susceptibility versus temperature were performed for at least one sample from 40 of the structures. Numbers of measured samples are listed in Table S1 (SupplementaryMaterialsA) and were 268 in total. Most obtained curves are characterized by irreversible behaviour (Fig. S1, SupplementaryMaterialsC). About half of them are similar to the curve shown in Fig. 4 (upper left, BP217). Until about 400 °C susceptibility remains constant or decreases slowly. Between 400 and 500 °C alteration starts and is indicated by a strong increase of susceptibility reaching a maximum above 500 °C. A contribution of the Hopkinson effect cannot be excluded. After this maximum the Curie temperature is approached around 580 °C indicating that the alteration product is a mineral close to magnetite. It is reasonable to assume that such an alteration took place already during heating in the past but it was not completed. Accordingly, the magnetic carrier of the remanence is the same mineral. During cooling a moderate to strong enhancement of susceptibility is observed with respect to the initial value showing that the sample was not sufficiently heated to stabilize in the past. According to Kostadinova-Avramova & Kovacheva (2013) stabilization is better for many heating cycles and the higher the temperature was. Fig. S1 (SupplementaryMaterialsC) shows that the behaviour can be more or also less complex. A similar behaviour is also observed for all kinds of soils (Jordanova 2017) and magnetic enhancement can be much stronger than observed here. About one third of the examples (Fig. S1, SupplementaryMaterialsC) show a similar behaviour but here the heating curve has two or more local maxima or bumps in the temperature range from 100 to

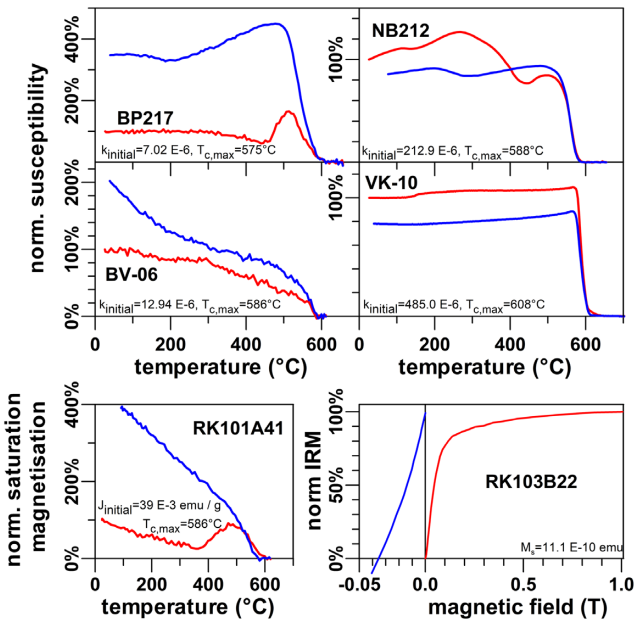

Figure 4. Diagrams of bulk susceptibility versus temperature normalized to the initial value with heating curves in red and cooling curves in blue (upper part and middle). The lower left diagram shows a result from a VFTB in the same manner, while the right part shows IRM acquisition (red) and back field curve (blue). Sample names, initial values and maximal Curie points are given (*cf.* Table 1).

400 °C as seen in the heating curve of Fig. 4 (upper right, NB212), here it is crossed by the cooling curve and only a moderate change of initial susceptibility is observed. The latter is interpreted as an indication that alteration was already almost finished in the original material. There are also samples which show such a heating curve, but here the cooling curve is always above the heating curve (Fig. S1, SupplementaryMaterialsC, DE_103_01).

A further type present in some samples (Fig. 4, middle left, BV-06) shows no indication of alteration during heating and Curie temperatures around 580 °C can be determined. Nevertheless, the cooling curve lies above the heating curve and a strong increase of susceptibility is present. Most of the investigated samples were baked clay or soil but the same behaviour is also observable for metamorphic rocks. The last example (Fig. 4, middle right, VK-10) shows a quite different behaviour with a continuous increase during heating due to a weak Hopkinson effect and Curie point above 600 °C. After heating some decrease of susceptibility is observed. Such curves were observed only for rock material like granite or gneiss and the high Curie point indicates that the magnetic carrier is maghemite. Fig. S1 (SupplementaryMaterialsC) shows also seven examples of almost reversible thermomagnetic curves (e.g. AT_003_04 or DE_116_01) and in some cases a clear indication of a Curie point above 600 °C is present (e.g. AT_003_04 or DE_125_01). Here hematite with impurities could also be present.

Fig. 4(lower left) shows an example of a thermomagnetic curve of saturation magnetization obtained from a VFTB. Such curves were measured only for three structures (RK1, RK2, RKK, *cf.* Table S1, SupplementaryMaterialsA) and they all look very similar. They show clearly that alteration is starting around 350 °C and the Curie temperature is reached around 580–600 °C. After heating saturation magnetization shows a strong increase because of the alteration product being a mineral close to magnetite. The corresponding IRM acquisition and back field curves all look like the example shown in Fig. 4, (lower right). Here saturation is not reached around 0.3 T indicating that also high coercive minerals like hematite are present in these baked clays. This is not the case for two slag samples (SE8,9, *cf.* Table S1, SupplementaryMaterialsA) which reached saturation.

Although the provided examples do not cover all sites it can generally be assumed that the magnetic carriers are iron-oxides which were mainly formed during heating of the feature (e.g. Kostadinova-Avramova & Kovacheva 2013; Jordanova 2017). The final drop at ∼580 °C seen in almost all curves is indicative for a mineral close to magnetite (Dunlop & Özdemir 1997). Susceptibility decay observed at much lower temperatures can be interpreted as the presence of instable maghemite, which is altered to magnetite or hematite (Hanesch *et al.* 2006; Jordanova 2017). Heating was often not high or long enough to complete alteration of other iron rich minerals. Frequently, also a contribution of a high coercive mineral, presumably hematite, is present to some extent, which was seen during AF demagnetization (see below). For strongly baked material, for example pottery kilns or bricks, hematite may dominate the magnetic properties as indicated by high median destructive field values, even lying above the maximum AF demagnetization field.

5.2 Stability of NRM

For all specimens natural remanent magnetization, bulk susceptibility and mass were measured. The distributions of NRM directions varied from very well confined (8.6 per cent of structures) to very scattered (7.8 per cent). Normally the NRM directions were confined (57.8 per cent) but some outliers or scatter were present. The rest of structures showed elongated distributions or a few clusters (6.3 per cent) or directions were scattered (19.5 per cent) without a clear concentration.

The Koenigsberger factor (Q-ratio; Koenigsberger 1936) shows the trend to increase with susceptibility and NRM intensity in the same way as shown by Schnepp *et al.* (2004). Normally a large variation of NRM intensities and bulk susceptibilities over several orders of magnitude is observed (Fig. 5) although similar ranges are observed for weakly baked material like burnt layers, hearths, fireplaces or roasting pits in comparison with well heated features like smelting furnaces. The large distribution of values is especially caused by the block sampling technique, because the outer (or lower), systematically less heated parts of the features are also sampled. This is supported by the much more confined distribution of values, for example shown in fig. 4a of Schnepp *et al.* (2015) which exclusively used the soft core technique. Furthermore, the well heated features have higher Q-ratios (Fig. 5, e.g. SE) while values between 1 and 5 are most frequent. Nevertheless, such values indicate the thermal overprint and that the NRM is at least a partial thermoremanent magnetization (pTRM). Accordingly, for structures with well concentrated NRM directions (about 66 per cent) and Q-ratios above 2 alternating field (AF) demagnetization was preferred. For sites sampled with blocks, in most cases two specimens were subjected to AF and one to thermal demagnetization. For soft cores, depending on length of the core AF, thermal or both demagnetization techniques have been applied to one or two specimens per core. For structures built with brick and/or rocks (13 per cent) multicomponent thermoremanent magnetizations (TRM) were expected and accordingly thermal demagnetization was preferred, but except for two cases AF demagnetizations were also performed routinely.

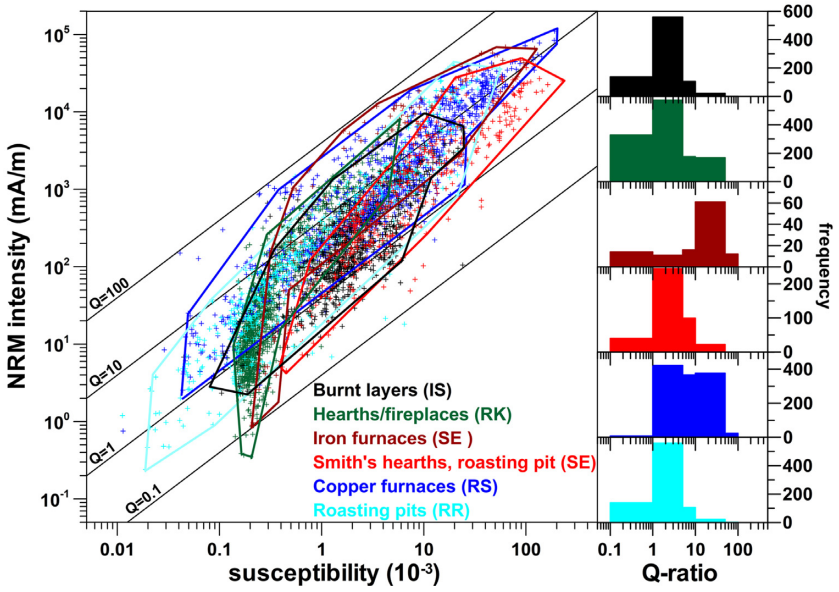

Figure 5. The intensity of natural remanent magnetization (NRM) is plotted versus bulk susceptibility, all values were normalized to a mass of 20 g, isolines of Koenigsberger ratio Q are shown. The data from the locations Isingerode (IS), Rodenkirchen (RK), Semlach (SE), and Eisenerz S1 (RS, RR, *cf.* Table 1) are shown in different colours and the main concentration is surrounded by a line. Histograms of the Q-ratios are shown at the right.

5.3 Demagnetization behaviour

In most cases the Thellier viscosity tests provide values of 10 per cent or less while about 20 per cent of the specimens give values of 10–30 per cent or even higher (5 per cent of the specimens). This implies that predominantly weak but also considerable viscous overprints have to be expected. Representative examples of the demagnetization results are given in Fig. 6 for thermal as well as alternating field treatment. For the majority of the structures the directional behaviour of the specimens during AF demagnetization was simple and easy to interpret, because only weak sometimes even no viscous components had to be removed.

Fig. 6(a) shows such an example of perfect behaviour from a Roman praefurnium of a hypocaust (Table 1: AT_020_01, RZ3), which had been built with local rock material. Here no secondary components are present and the directions of specimens from the same sample agree very well. Such a very good demagnetization behaviour was found for 20 of the sites (*cf.* Table S1, SupplementaryMaterialsA, column AI).

In about half of the structures weak secondary components are observed which were easy to remove. The majority of the specimens showed demagnetization behaviour as seen in Fig. 6(b), which is an example from an Early Medieval pottery kiln, made from baked clay (Table 1: DE_106_01, BW1). The demagnetization was performed with narrow steps and shows a small viscous overprint which is removed by 10 mT or 150 °C, respectively. Then well-defined straight lines to origin are obtained, which give very similar directions for both demagnetization procedures. Generally thermal demagnetization was noisier. Thermal demagnetization series were more difficult because reheating of weakly baked material made the specimens brittle and could have caused chemical alterations which disturb the demagnetization lines.

For many structures sampling comprised also rocks or bricks which had not been sufficiently reheated to replace the original NRM. So, two TRM components were present. Often, they could be separated by AF demagnetization, but also great circle behaviour was observed notably for specimens which carried a pTRM overprint. Here it was easier to separate different magnetic components by thermal demagnetization and it was preferred for about 18 per cent of the structures (see Table S1, SupplementaryMaterialsA). The example (Fig. 6c, Table 1: DE_116_05, MY4) was taken in a castle from a Modern Age fireside which was made of bricks. The pTRM overprint due to heating during use of the structure was identified as characteristic remanent magnetization (ChRM) direction in the low temperature range. After removing a small viscous component, this overprint is seen as well-defined straight lines which were approximately parallel for all specimens. At higher temperatures the original magnetization of the brick is seen during thermal demagnetization, but it could not be identified with AF demagnetization, because the carrier is magnetically hard. For six specimens great circles had to be used to obtain the ChRM (Fig. 7). Such a good demagnetization behaviour (Figs 6b and c) predominated 91 of sites (*cf.* Table S1, SupplementaryMaterialsA, column AI).

A typical example from a burnt soil layer taken from a hill fort of late Bronze Age (IS4) is illustrated in Fig. 6(d). This was a bit more difficult to interpret, because the specimens show a somewhat scattered behaviour or several components. Relatively strong overprints were removed at 30 mT, while thermal demagnetization data points scatter below 300 °C and above 500 °C thermal alteration leads to a distortion from the stable direction. In two cases completely unstable demagnetization behaviour and no line towards origin was observed (Fig. S2, SupplementaryMaterialsC). Nevertheless, most specimens show a good agreement of their stable directions. Therefore, also a weakly burnt layer can provide a reliable secular variation signal.

Fig. 6(e) shows results from a Late Roman oven or hearth (HB2), which was paved with local limestone plates, with rather low NRM intensities and susceptibilities. Here AF demagnetization was noisy because of the weak intensity and a secondary component is present (HB217A11). The surrounding baked clay (HB202A) shows only a partial TRM with some overprint at the beginning but then sufficient data points for principal component analysis. A secondary compo-

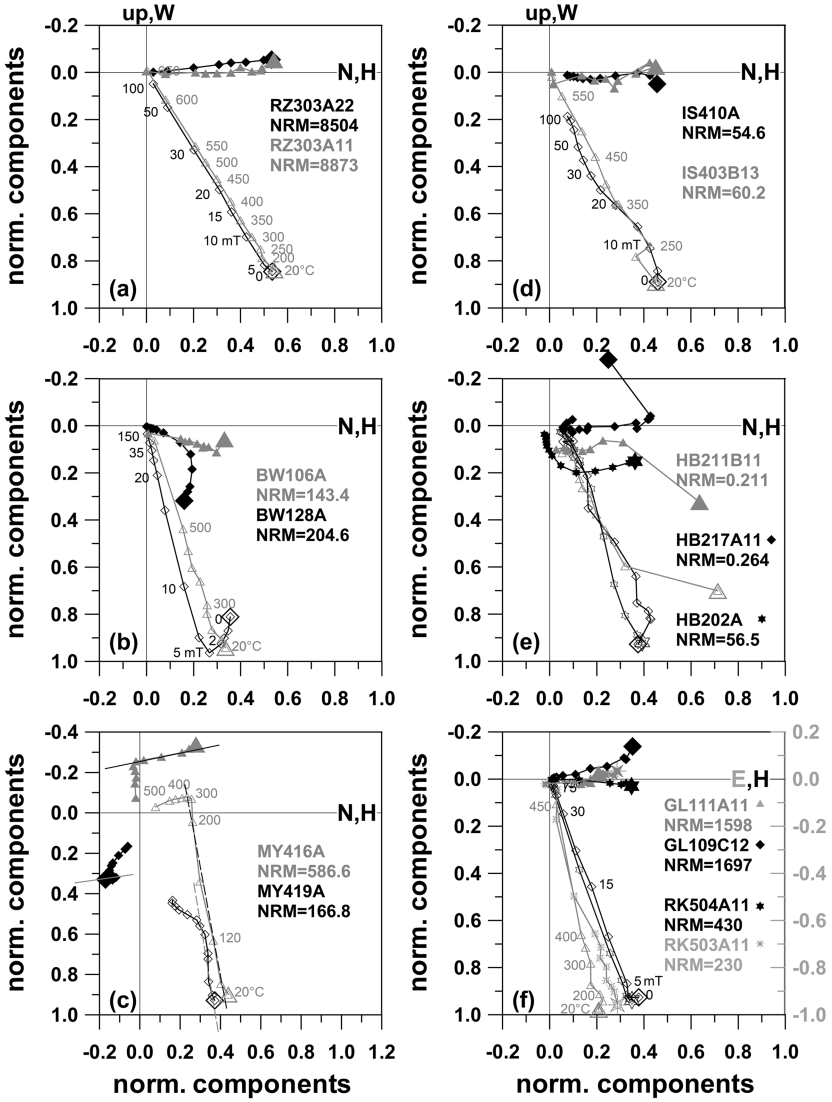

Figure 6. Diagrams of normalized orthogonal components of demagnetized specimens from several new structures (cf. Table S1, SupplementaryMaterialsA), grey symbols show thermal, black symbols AF demagnetization. Closed symbols are Y component (W-E, ordinate) versus X component (N-S, abscissa, corresponds to declination), open symbols are vertical component (up-down) versus horizontal component (H, corresponds to inclination). Specimen names and NRM in mA m^{-1} are given, and numbers indicate temperature or AF steps. Note that in (f) the X-Y plane is rotated with respect to the other diagrams (W-E, abscissa).

nent is seen during thermal demagnetization (HB211B). Alteration is indicated by the last temperature step (500 °C). Many specimens from this archaeological feature had unstable remanences, but finally a well-defined mean ChRM was obtained including two great circle results (*cf.* Table S1, SupplementaryMaterialsA: AT_004_02).

When the demagnetization behaviour of a site was mainly like the examples shown in Figs 6(d) and (e), but also good behaviour was obtained, the overall behaviour was classified as passable and 46 sites fall in this category (*cf.* Table S1, SupplementaryMaterialsA, column AI). The category poor was attributed to 6 sites (*cf.* Table S1, column AI), because the demagnetization behaviour was mainly only passable, agreement on sample level was not good, and a considerable number of specimens with unstable behaviour was present. The last examples (Fig. 6f) are taken from two structures which are not very well dated just before the turn from Bronze to Iron Age. One (GL1) was the remains of an oven of unknown use, while the other was a hearth found in an excavated house (Rodenkirchen, see above). The four examples show only weak overprints and very stable demagnetization behaviour. So, both sites showed a good demagnetization behaviour (*cf.* Table S1, SupplementaryMaterialsA, column AI). Directions within as well as between the structures are very similar, but somewhat unusual, because declination points almost to the East, while inclination is as steep as expected for the past 2500 yr (see Schnepp & Lanos 2005).

Apart from the examples shown here, additional demagnetization series can be found in several other publications (Klemm *et al.* 2005; Aidona *et al.* 2006; Trapanese *et al.* 2008; Schnepp 2008a,b, 2010a,b, 2011a,b, 2015, 2016, 2017, 2018; Schnepp & Brüggler 2016; Schnepp *et al.* 2016). They also provide preliminary mean directions which are supplied with the new data and updated here.

Generally, most specimens showed well defined single or two component magnetization systems and clustered ChRM directions. Nevertheless, about 12 per cent of all demagnetization experiments

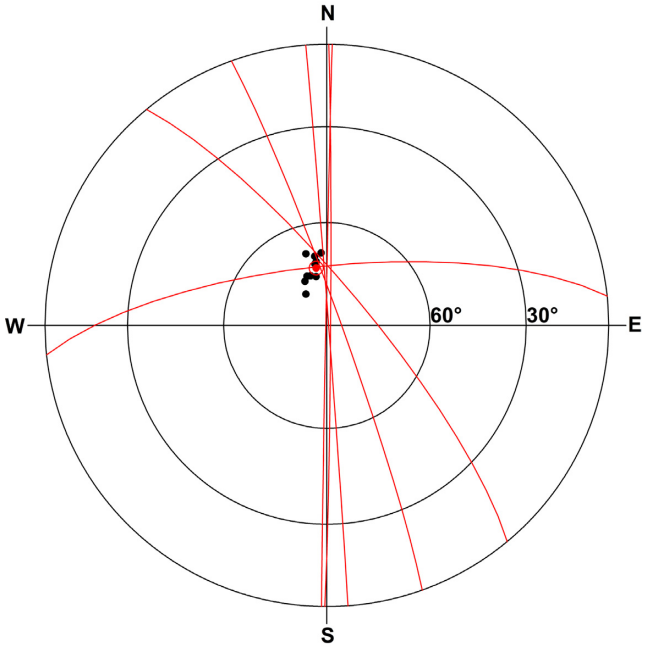

Figure 7. ChRM directions (dots) and great circles (red lines) in stereographic projection of a modern fireplace (ingle) in Meyenburg castle (MY4, Table S1, SupplementaryMaterialsA). The mean ChRM is shown as red dot with its confidence circle.

revealed unstable behaviour and for many (37 per cent) of the structures this behaviour was seen for more than three specimens (see Table S1). This happened, for example for material which was not well compacted (e.g. DE_109_01, Table S1, SupplementaryMaterialsA or AT_003_07; Schnepp 2017), disturbed by bioturbation (e.g. wormholes filled with other material, site DE_104_01, Table S1, SupplementaryMaterialsA) or having a sandy character (e.g. Table S1, SupplementaryMaterialsA: DE_113_01; Schnepp & Brüggler 2016; DE_101_01; Schnepp 2010a). Nevertheless, a considerable number of unstable specimens do not necessarily corrupt success of archaeodirection determination when many samples had been taken (e.g. Table S1, SupplementaryMaterialsA, AT_009_03). Such unstable magnetization behaviour was also seen, for weakly burnt structures like incidence layers, seldom used fireplaces or magnetically weak material like limestone or dolomite. However, specimens exhibiting such unstable magnetizations dominated only in a few cases the demagnetization behaviour of a structure and therefore in most cases the ancient field direction could be retrieved, unambiguously.

5.4 New archaeomagnetic directions

ChRM directions have been obtained by principal component analysis (Kirschvink 1980) from the demagnetization experiments. Sometimes also strong secondary components have been observed, mainly in strongly magnetized structures like smelting furnaces or pottery kilns. Although a considerable part of demagnetization experiments dealt only with a partial TRM in most cases the components were clearly separated. For 18 structures (and 6 updated, see below) also great circles have been used (e.g. Fig. 7, Table S1, SupplementaryMaterialsA) but they comprise less than 2 per cent of all ChRM results. In 6 cases (and 3 updated, see below, Table S1) following Thellier (1981) the viscosity cleaned NRM obtained from the viscosity tests have been used as 'ChRM' direction.

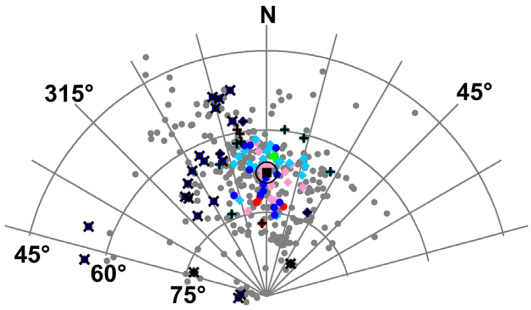

Figure 8. Stereographic projection of NRM (grey) and ChRM directions of twin furnaces RS1 (blue/light blue) and RS2 (red/rose) from Eisenerz (Table S1, SupplementaryMaterialsA). Dots indicate rock samples, while diamonds are baked clay, ChRM directions which were tested (+) and rejected (X) as outliers are marked by crosses. The mean ChRM is shown as a black square with its confidence circle. The present field direction is plotted as a green star.

Outlier tests according to McFadden (1982) have been performed in total for 72 (44 per cent, cf. Table S1, SupplementaryMaterialsA) structures for the following reasons: (a) Results of material, which was suspected to be displaced (e.g. bricks, tiles: Table S1, SupplementaryMaterialsA, DE_126_01, NO; rocks: AT_008_02, RS1,2; potsherds: AT_002_01, ST1) or deformed (cupola of DE_121_01, NB1), (b) which was not sufficiently heated or (c) which may not belong to the structure. Additionally (d), very short soft cores were tested, because their orientation was difficult and may have a large error (e.g. Table S1, SupplementaryMaterialsA, DE_108_01, SI). Moreover (e), results of those specimens were tested, which were deformed by little pebbles or scrunched (Table S1, SupplementaryMaterialsA, DE_130_04, IS). Furthermore (f), the directions obtained from the viscosity test were checked systematically because some of the specimens had viscosity indices exceeding 15 per cent. Finally (g), ChRM directions identified during Thellier experiments (26 structures, Table S1, SupplementaryMaterialsA) were systematically tested as outliers in order to check their correctness because a distortion of direction may arise from chemical alteration (Hervé *et al.* 2011) or it may come from the specimen preparation as small cubes that have been cut from larger ones or from cylindrical specimens.

Finally, 182 directions on specimen level were removed as outliers from the data sets (2059) of 58 structures (40 per cent). But only 15 (12 per cent) structures had a considerable number (>3) of outliers. The largest numbers of outliers were obtained for the cupola of an iron smelting furnace (Table S1, SupplementaryMaterialsA, DE_121_01, NB1) that was deformed after cooling and the rocks of a copper smelting furnace (Table S1, SupplementaryMaterialsA, AT_008_02, RS1,2) which were moved by roots of a tree.

The latter is shown in Fig. 8 as an example for the application of outlier tests. The NRM directions of these twin furnaces are very scattered and somewhat elongated but the centre of concentration does not coincide with the present field direction. Apart from this, some clusters are seen lying far away from this centre. After demagnetization the directions and their distribution do not change much. Then the outlier test was done in two steps: 1. All results from rock samples which were suspected to be displaced were tested as outliers and the result was negative (seen in the left part of Fig. 8). 2. After excluding them all results lying on the rim of the main concentration were subjected to the outlier test and only two results from the baked clay were not accepted. Finally, the hierarchical mean based

on 27 samples gave a very well-defined mean significantly different from the present field direction.

According to Kovacheva *et al.* (2009) no systematic tests of magnetic anisotropy seemed necessary because the sampled material was mainly baked clay. Investigations of susceptibility and/or TRM tensors were done only for four structures (Table S1, SupplementaryMaterialsA: AT_003_01–AT_003_03, AT_012_02,) and applied only in one case. They were chosen because the building material comprised metamorphic rocks like Gneiss or Schist, which showed strong anisotropy. Only in one case the correction of anisotropy was finally applied and changed the direction significantly (Schnepp 2017), while for the others no change in direction but enhancement of scatter was observed.

An indispensable requirement for obtaining a correct reading of the archaeomagnetic field directions is that the structure did not move since its last cooling. This premise seems not to be fulfilled by the piles of hearths seen in Fig. 3 of the Late Bronze Age house in Rodenkirchen (RK). They are obviously tilted, and it seems unlikely that they were used in this position. Tilting of the structures is very likely because the wharves underlying the settlement area were themselves placed on the young fluviatile sediments of river Weser. Fortunately, during the excavation, a very precise 3-D survey of all features was undertaken and data of the rims of the hearths and fireplaces were kindly provided by the archaeologists. From these data tilting and bedding correction parameters were calculated by assuming that the feature was circular with the rim lying in the horizontal plane. Dip angles ranging from 1.2° to 5.5° were obtained and applied to the mean directions. The results (Fig. 9) show that after bedding correction the scatter between directions is considerably reduced but most structures still have unusual eastern declinations with values between 30° and 60°, while the observed inclination remains relatively steep. The only direction within the range of known secular variation of the past 2500 yr is the fireplace RK3 used in the youngest phase of occupation. NRM directions of each Rodenkirchen structure were mostly well concentrated, weak secondary overprints were easily removed and no unstable behaviour was observed. As the material had been very brittle and consolidation and cutting was difficult the shape of the cubic specimens was often not ideal. The outlier test removed some aberrant directions. With respect to NRMs a better concentration of ChRM directions was observed. Precision parameter values (Fisher 1953) range from 116 to 643 and α_{95} angles between 1.6° and 4.5° (*cf.* Table S1, SupplementaryMaterialsA: DE_129_01–DE_129_12) were obtained. Overall, the directions of Rodenkirchen are of good quality and they are judged to be reliable.

The mean direction for each structure was calculated in a hierarchical process by averaging first on sample and then on structure level. They are listed in Table 1. In 15 cases a joint mean of all samples from two or more structures of the same age was calculated (see Table S1, SupplementaryMaterialsA, e.g. DE_113_01: GA1,3; Schnepp & Brüggler 2016 or AT_009_03: KB2,3,7; Schnepp 2011b) indicated by a name with comma or hyphen. The overall archaeodirectional data quality can be accessed by the parameters obtained from the Fisher statistics (Fisher 1953) like confidence circle's radius α_{95}, precision parameter k and the number of independent samples that was at least five. Fig. 10 shows histograms of these parameters. α_{95} values range from 1.4° to 9.2° and about half of the structures have very well confined mean directions with α_{95} less than 3° while only 11 exceed 6°. The k values range from 9 to 1369. Mostly they are also very good and only for 7 structures they are below 50. The overall good quality of the archaeodirections could be achieved by a large number of samples which was below 10 only for 32 structures and very often above 15 (52 structures).

Nevertheless, nine of the results are classified as unreliable for the reasons documented in column 'Remarks' of Table S1 (SupplementaryMaterialsA). For structures RSL, THM, SE2, SEJ, SF and GA2 (Table S1, SupplementaryMaterialsA: AT_007_01, AT_010_13, AT_003_02, AT_003_07, DE_109_01 and, DE_113_02) explanations were given already in the corresponding publications (Klemm *et al.* 2005; Schnepp 2015; Schnepp *et al.* 2015; Schnepp & Brüggler 2016; Schnepp 2018).

Structure BN (see Table S1, SupplementaryMaterialsA: AT_013_01) consists of two superposed pottery kilns of Roman age according the archaeological designation. NRM directions showed much scatter but a clear concentration at relatively steep inclinations. The demagnetization behaviour was in most cases simple and only weak secondary components were removed. It confirmed the relatively steep inclination at 79° which is about 15° steeper than the one expected for the 1st century AD. A tentative dating using the 2015 Austrian curve (Schnepp *et al.* 2015) lead to an age encompassing the 7th and 8th centuries AD. Although the statistic parameters of the direction are not particularly bad the result has to be treated with caution because of the uncertain age until a better age estimation may be available.

Structure SLW (Table S1, SupplementaryMaterialsA: AT_016_01) merges results from contemporaneous iron furnaces and a burnt castle wall of late La Tène Age. NRM directions were very scattered and clusters were only seen for specimens from the same block. Demagnetization behaviour was poor and did not reduce the scatter. Amphibolite blocks were used as building material for the furnaces and this rock also was present as debris all over the site. This rock is strongly magnetic and anisotropic, but no correction was performed. For these reasons and because of possible displacement of the blocks the mean direction is not reliable, further supported by the very low precision parameter.

Structure LE (Table S1, SupplementaryMaterialsA: AT_017_01) was a very precisely dated bell mould erected with local rubble stone embedded in clay which was sampled as drill cores and oriented blocks. NRM directions were rather scattered and not much confined after demagnetization. Only three samples have very similar directions, but application of an outlier test seemed not appropriate. The obtained precision parameter is rather low (38) and inclination is much shallower than expected for the 17th century. The large dispersion is very likely caused by movements of the rounded blocks. Accordingly, this result is not reliable.

The site Wörterberg (Table S1, SupplementaryMaterialsA, AT_014_01: WB1, AT_014_02: WB2) is an example for a very large time gap present between two directly superimposed structures, which were originally considered as contemporaneous. Based on a few potsherds found in the structure and other Roman sites in the vicinity the kilns were attributed as Roman pottery kilns dating into the 2nd to 3rd centuries AD (Krenn 2007). Preliminary results seemed to confirm this by the archaeomagnetic direction of the upper kiln (Trapanese *et al.* 2008). But further measurements show that the two kilns have directions (Fig. 11) which are significantly different from each other according to an F-test (McFadden & Lowes 1981). Further inspection of the archaeological assemblage concluded that the older structure was a late Roman pottery kiln which was corroborated by potsherds while the younger structure was a modern age brick kiln charted in a military map from 1869 and supported by the fact that it is still in the knowledge of elderly

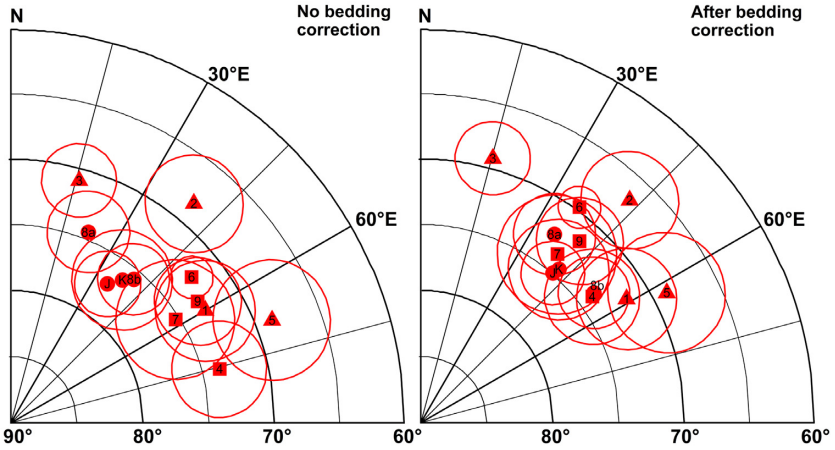

Figure 9. Results from Rodenkirchen (RK, Table S1, SupplementaryMaterialsA). Mean characteristic remanent magnetization directions (red) together with α_{95} are shown in stereographic projection before (left) and after (right) bedding correction. Data come from the central (squares) and the second pile (dots) inside the house and from the fireplaces (triangles) situated on plateaus.

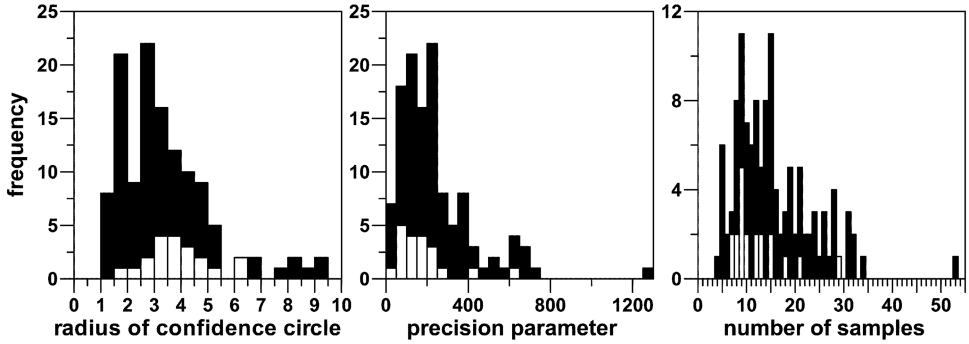

Figure 10. Histogram of the (Fisher 1953) statistics parameters obtained for 121 structures. Parameters of 20 structures with unusual directions are shown by white bars.

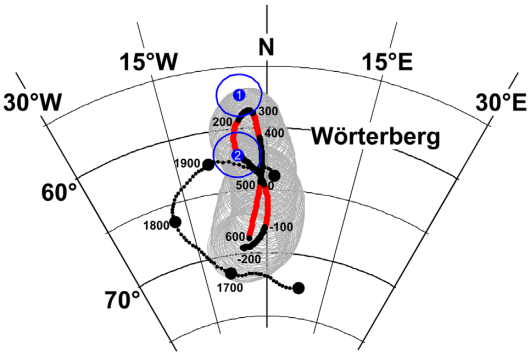

Figure 11. Mean ChRM directions with confidence circles of the superimposed kilns from Wörterberg (in blue, 1: lower, 2: upper; Table 1: WB) in comparison with the Austrian archaeomagnetic reference curve (Schnepp & Lanos 2006) and the historical SV curve (GUFM, black dots; Jackson *et al.* 2000). Numbers indicate years AD.

people living in the area (E. Szameit, Vienna, personal communication 2017). The obtained directions are in perfect agreement with the dating (see Table S1) as shown in Fig. 11.

In some cases, the archaeologists could only provide a rough age estimate of the investigated structure (Table S1, SupplementaryMaterialsA: DE_110_02, DE_123_01, DE_128_03). While the presumed age of the first two structures lies in times BC and no precise calibration curve is available for these times, which is supported by a sufficient regional database, archaeomagnetic dating for the third structure was already provided by Schnepp (2016).

5.5 Updated published data

Apart from the above-mentioned updated age information (Table 3) with respect to published data directions of eight Austrian and ten German features have also been updated (see Table 3). This happened because further sampling had been undertaken, sometimes more structures with the same age were sampled (*cf.* for example #147 (BR1) in table 2 of Schnepp & Lanos 2005 with DE_087_01: BR1–4 in Table 3) or because new results of demagnetization measurements were added (e.g. #3 in table 2 of Schnepp *et al.* 2006 and AT_002_02: ST2 in Table 3). Furthermore, for eight structures directional results from palaeointensity experiments were added (*cf.* Table S1, SupplementaryMaterialsA, column PIdemag). All updated directions are given in Table 3. The change in direction was in the order of 1° or less with only two exceptions (AT_004_01 and DE_087_01 in Table 3) which were combined with results from more structures. Here change was larger than 2° but still smaller than the α_{95} of the published direction. Accordingly, no significant changes in direction were observed, α_{95} decreased and the precision parameter k increased in most cases. Another exception is a charcoal pile (AT_007_01 in Table 3), which was sampled independently

two times (Klemm *et al.* 2005, 2017) for the purpose of archaeomagnetic dating. Both studies were re-evaluated and combined. The final directions have overlapping α_{95}-circles.

5.6 Archaeomagnetic dating

As an example of application of archaeomagnetic dating results of two structures from Eisenerzer Ramsau (see Tables 1 and 3, AT_026_01: LM2, AT_007_1: RSL) with only poor or passable demagnetization behaviour are provided here (Figs S3 and S4). The last usage of two charcoal piles (RSL and LM2) has been investigated in the Eisenerzer Ramsau (see above, Klemm *et al.* 2005, 2017). Because the structures are expected to have modern age the secular variation reference curves derived from global field predictions (BIGMUDI4k.1, Arneitz *et al.* 2019) are used. This model (available at http://cobs.zamg.ac.at/data/index.php/en/data-access/geomagnetic-model) is based on a combined data set of archaeomagnetic and volcanic records (e.g. Brown *et al.* 2015) as well as historical measurements (e.g. Jonkers *et al.* 2003) compiled within the HISTMAG database (Arneitz *et al.* 2017b). Very accurate dating of one structure was not possible due to a rather high α_{95} value (Table 1, Fig. S4, SupplementaryMaterialsC). While for this structure (LM2) various periods are possible including that of the archaeological dating, RSL was most likely in use for the last time around the end of the 19th century (Fig. S3, SupplementaryMaterialsC). This agrees well with the independent temporal classification of the studied charcoal pile type (Klemm *et al.* 2017), which is based on archaeological and historical evidence. This shows that also low-quality data can provide reasonable results but should be treated with caution.

5.7 Data sets

The new data set from Austria was updated with new data comprising 14 already published directions (Schnepp *et al.* 2015), 7 revised directions together with 45 directions obtained at eight Austrian sites, where sampling had been continued and further 17 new directions from features at 14 new sites. Seven of these directions are classified as unreliable for the reasons given above, while the rest is considered as a reliable measure of the Earth's magnetic field attributed to the last heating of the structure. The total data set for Austria comprises now 85 archaeodirections covering the time interval from the middle of the Bronze age to recent ($\sim$ 1600 BC to $\sim$ 1900 AD).

The data set of Germany (Schnepp & Lanos 2005) is supplied with 3 revised ages, 10 revised directions and 65 new directions obtained from 31 new locations. Only two directions are not reliable as explained, for example in the corresponding publications (Schnepp 2016; Schnepp & Brüggler 2016), but three directions come from poorly dated features with age errors of 1000 yr or more. The total German data set comprises now 225 archaeodirections covering the time interval from the end of the Copper age to recent ($\sim$ 3500 BC to $\sim$2000 AD) but times before 1000 BC are very sparsely covered.

Two directions from Switzerland are also presented which can be added to a data set of 24 directions found in the GEOMAGIA50 database (Brown *et al.* 2015).

6 DISCUSSION AND CONCLUSION

Fig. 12 shows the new data in comparison with the published secular variation reference curves for Austria and Germany (Schnepp & Lanos 2005, 2006). Note, that the curve for Austria was based on only 9 sites from Austria, while 185 data came from the surrounding countries. The data are reduced to the respective reference point. Results dating before 1600 BC were omitted as well as three German directions with a rather large dating error (Table 1). In both cases the new data are generally in good agreement with the published curves which rely apart from revised data (7 for Austria and 12 for Germany) on independent data sets including also directions from the surrounding countries. Data which were classified as unreliable for independent reasons, obviously do not agree with the curves (open symbols). Some disagreement is seen for the inclination minima which occurred between 200–300 AD (Roman) and 1200–1400 AD (Medieval). In the new data set from Austria minimal inclinations cluster around 400 AD (*cf.* red data points in the upper inclination diagram of Fig. 12) and do not coincide with the minimum of the curve. For the Medieval minimum disagreement is seen for the new data from Germany (*cf.* purple data points in the lower inclination diagram of Fig. 12) and the curve of Schnepp & Lanos (2005). Here the little bump seen around 1300 BC is not supported by the new data. Accordingly, new calculations of the secular variation curves will be necessary.

While the geographic distribution of sites in Austria (Fig. 1) tends to be more even, in Germany a bias of sites is seen in the northern part and the Rhineland. Also, the temporal distribution of data still prefers time intervals with frequent excavations like the Roman or Medieval Ages (Figs 12 and 3) but a good progress was made to fill gaps, for example in early Medieval time. Some new data also cover the important time interval in which archaeomagnetic data overlap with the oldest direct observations of the geomagnetic field (see e.g. Arneitz *et al.* 2017a,b). An important progress made by this work is also that a reasonable number of directional data have been obtained from the time interval 1500 to 0 BC which is characterized by very large variations of archaeointensities (Hervé *et al.* 2017) and may play a key role for understanding enhanced secular variation.

Such an enhanced secular variation is also seen in the directional data set presented here. All archaeomagnetic directions obtained in the time interval 1200 to 500 BC have eastern declinations with values up to about 70°. A considerable part of them exceeds even the maximum declinations of 30–40° obtained by Hervé *et al.* (2013) for France (*cf.* directions of AT_022, AT_023, DE_128, DE_129, DE_130 in Table 1). Inclinations are often relatively steep but with values between 60° and 75° they are in agreement with the normal range of secular variation (*cf.* Fig. 12).

For specimens with unusual results stable directions have been obtained during demagnetization experiments (Figs 6d and f), as discussed above. Only for site Isingerode (Table 1, DE_130) unstable demagnetization behaviour was observed because the in situ burnt soil was interspersed with many pebbles, which were not sufficiently heated. For site Maukental (Table 1, AT_023) the remanence had very low magnetization intensity as it was recorded by dolomite debris heated by fire setting in a Bronze Age mine. During the rescue excavation at Glocksin (Neutzer 2003; Table 1: DE_128) a structure of an oven was sampled, which showed two distinct directional clusters. The excavation revealed two pits and one was identified as an oven, but the two phases of use identified by palaeomagnetism were only recognized after further inspection. The neighbouring pit contained pottery which was classified as Late Bronze to Early Iron age and late Neolithic. A sample of charcoal was taken from outside of the oven's rim. The calibrated age is compatible (see Table S1, SupplementaryMaterialsA) with the dating of the potsherds but may not be directly associated with the use of the ovens. Therefore,

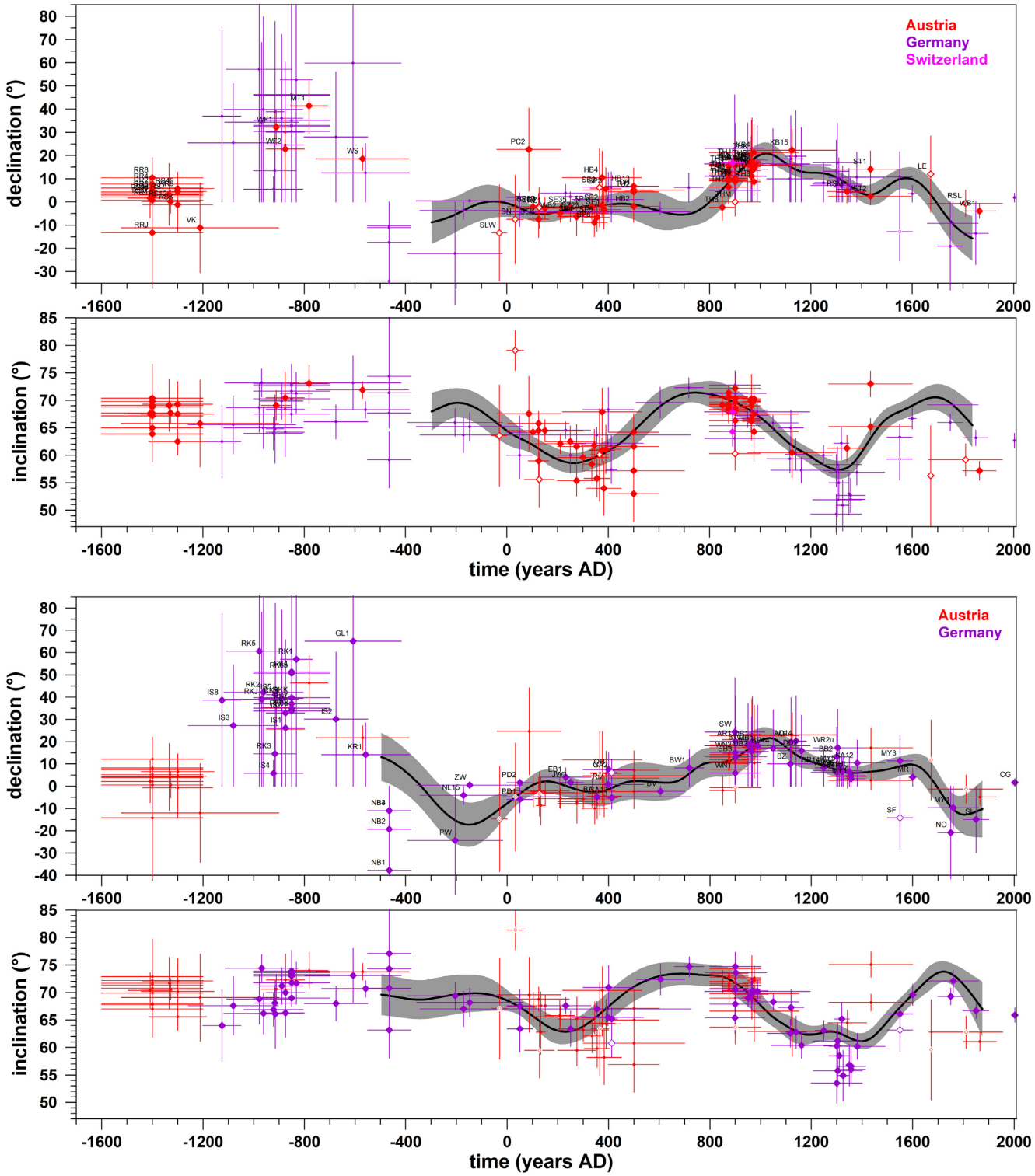

Figure 12. Declination and inclination values from Austria and Germany are plotted versus time together with their error limits (Table 1), unreliable data are indicated by open symbols. Upper diagrams: All data are reduced to Radstadt, the reference point of the secular variation curve of Austria (Schnepp & Lanos 2006) and plotted with the Austrian reference curves. Lower diagrams: Data are reduced to the German reference point Göttingen and the secular variation curves of Germany (Schnepp & Lanos 2005) are shown. These marginal curves are shown as bold black lines surrounded by their 95 per cent error envelope (grey area).

for the lower feature as assigned age the one of the locality was preferred, although the error interval is rather large so that the direction is not plotted in Fig. 12. The demagnetization behaviour of the upper part with unusual direction was good (Fig. 6f, Table S1, SupplementaryMaterialsA) and two well distinct directions were obtained.

The demagnetization quality of the 20 sites with declination values above 25° is very good for 1 site, good for 14 sites, passable for 4 sites, and poor for only 1 site (*cf.* Table S1, SupplementaryMaterialsA). So, generally no special demagnetization behaviour of all these features has been observed. Although the ChRM directions are scattered the parameters obtained from the Fisher statistics are not particularly bad (see Fig. 10): The number of samples is between 7 and 29, k is between 45 and 643 and α_{95} is between 1.6° and 6.5°. For site Rodenkirchen (DE_129) it was also shown that the observed tilting of the structures would not explain the unusual directions because the declinations remain to be above 30°. Furthermore, a tilting of about 15° or a rotation by 40° or more would be needed to explain such unusual mean directions. It seems very unlikely that such a disturbance for so many structures remained undiscovered. Therefore, disturbances at site level seem unrealistic to account for these unusual directions. The ages are spread over a relatively long time interval, but the archaeological age estimates attribute all the features to the transition from Bronze to Iron Age. For about half of the structures the archaeological age estimate is supported by radiocarbon dating (see Table 2). Generally, precise archaeological age estimates for the transition from Bronze to Iron Age are difficult, but five sites are attributed more precisely to late Urnfeld or early Hallstatt Age.

The five sites with unusual directions are spread over the investigated area of Austria and Germany (Fig. 1) and the four multilevel sites comprise also features with directions within the range of 'normal' secular variation supporting further that reliability of the 20 unusual directions is not questionable.

Eastern declinations with values above 40° are also observed e.g. in France (Hervé *et al.* 2013), in Britain (Batt *et al.* 2017), in Italy (Tema *et al.* 2006), in Ukraine (Burlatskaya *et al.* 1986) as well as in Scandinavian lake sediments (e.g. Nilsson *et al.* 2018) in the time interval from 850 to 500 BC. In order to investigate this further all (90) data for a circle of 2000 km around a common reference point (Nürnberg: 49.5°N, 11.1°E) have been extracted from the HISTMAG database (Arneitz *et al.* 2017b, http://cobs.zamg.ac.at/data/index.php/en/data-access/histmag) for the time interval from 1600 to 500 BC. They were reduced to Nürnberg and they are plotted in Fig. 13 together with our new data. Additionally, a secular variation reference curve obtained from the BIGMUDI4k.1 model (Arneitz *et al.* 2019) is shown. The new Austrian and German data show a remarkable agreement with the trends of data points from other countries as well as for the curves. While there is little variation in inclination all data show a big movement of declination to the East but the amplitude for this oscillation is strongly underestimated by the model curve. So, the new directional data from Central Europe support that a strong movement of the Earth's magnetic field direction occurred at the transition from Bronze to Iron Age. This enhanced directional secular variation corresponds well with strong variations of the archaeointensity observed in Bavarian pottery in the time interval from 1000 to 300 BC (Hervé *et al.* 2017). Here a pronounced minimum is seen at 800 BC (less than 50 μT intensity) followed by a maximum at 650 BC (more than 80 μT intensity). The whole phenomenon needs further investigation. Further discussions on its nature or possible connections of the directional variation to other intensity highs observed, for example in Syria (Gallet *et al.* 2014) or the Levant (Shaar *et al.* 2016) are beyond the frame of this publication.

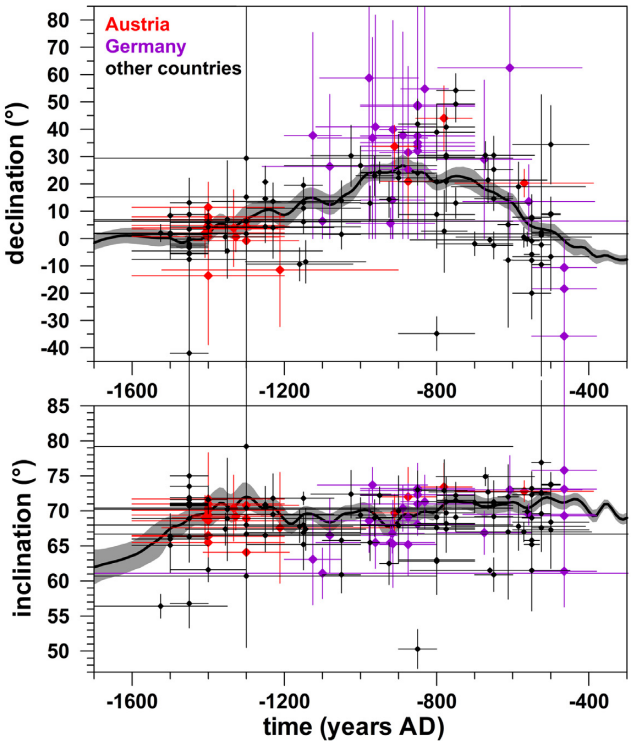

Figure 13. The same representation of the data as in Fig. 12, but they are reduced to Nürnberg (49.5°N, 11.1°E). All data available from the HISTMAG database (Arneitz *et al.* 2017b) for a circle of 2000 km around the reduction point are shown in black. The reference curve was obtained from the BIGMUDI4k.1 model (Arneitz *et al.* 2019, http://cobs.zamg.ac.at/data/index.php/en/data-access/geomagnetic-model).

The set of archaeomagnetic directions for Austria (85 sites) presented here was enlarged dramatically and is about fourfold with respect to already published data. The data set for Germany was increased by about 45 per cent to now 225 directions. The new data support the published secular variation reference curves of Austria and Germany of the past 2000 yr. A considerable number of data is presented for the time interval from 1500 to 500 BC and here a strong directional secular variation is seen. The data sets cover the past 3500 yr and will allow calculation of refined archaeomagnetic secular variation reference curves for central Europe.

ACKNOWLEDGEMENTS

We wish to thank all the numerous archaeologists who allowed for sampling at their excavations in Austria, Germany and Switzerland and provided information on the archaeological context and age estimation. By providing multilevel sites especially B. Cech, R. Gerlach, F. Glaser, S. Klemm, U. Müller, M. Obenaus, P. Scherrer, W.-D. Steinmetz, E. Strahl, G. Fleps and G. Wieland helped to increase the number of sampled structures, this is kindly acknowledged. Thanks to D. Dallaserra for providing the 3-D data of the Rodenkirchen hearths. E. Aidona kindly shared the raw data from Eisenerz. Many thanks to Y. Fleischhacker, F. Friedam, K. Gruber, M. Nievoll, A. Selge, W. Thöny, C. Zeeden (Leoben), R. Lubberich (Bonn), R. Pucher (Hannover), F. Mayrhofer (ZAMG), K. Worm and M. Klick (Grubenhagen) for help during field work, sample preparation and/or laboratory measurements. Some results

of radiocarbon or dendrochronological dating have been provided by the archaeologists, many thanks. For field work some financial support was provided by Archaeokontrakt (Berlin), LA für Denkmalpflege und Archäologie Sachsen-Anhalt, Rheinisches Amt für Bodendenkmalpflege and Landschaftsverband Westfalen-Lippe, RAB. The original manuscript benefited from the comments and suggestions of Wilbor Poletti and an anonymous reviewer. The study was supported by Austrian Science Fund (FWF): P19370-N19, P23295-N21 and P24722.

REFERENCES

Aidona, E., Scholger, R., Mauritsch, H.J., Schnepp, E. & Klemm, S., 2006. Spatial distribution of archaeomagnetic vectors within archaeological samples from Eisenerz (Austria), *Geophys. J. Int.,* **166,** 46–58.

Arneitz, P., Egli, R. & Leonhardt, R., 2017a. Unbiased analysis of geomagnetic data sets and comparison of historical data with paleomagnetic and archeomagnetic records, *Rev. Geophys.,* **55**(1), 5–39 (2016RG000527).

Arneitz, P., Egli, R., Leonhardt, R. & Fabian, K., 2019. A Bayesian iterative geomagnetic model with universal data input: Self-consistent spherical harmonic evolution for the geomagnetic field over the last 4000 years, *Phys. Earth planet. Inter.,* **290,** 57–75.

Arneitz, P. *et al.*, 2017b. The HISTMAG database: combining historical, archaeomagnetic and volcanic data, *Geophys. J. Int.,* **210,** 1347–1359.

Batt, C.M., Brown, M.C., Clelland, S.-J., Korte, M., Linford, P. & Outram, Z., 2017. Advances in archaeomagnetic dating in Britain: New data, new approaches and a new calibration curve, *J. Archaeolog. Sci.,* **85,** 66–82.

Biermann, F., 2010. Archäologische Studien zum Dorf der Ostsiedlungszeit. Die Wüstungen Miltendorf und Damsdorf in Brandenburg und das ländliche Siedlungswesen des 12. bis 15. Jahrhunderts in Ostmitteleuropa. Brandenburgisches Landesamt für Denkmalpflege und Archaeologisches Landesmuseum.

Bronk Ramsey, C., 2009. Bayesian analysis of radiocarbon dates, *Radiocarbon,* **51,** 337–360.

Brown, M.C., Donadini, F., Korte, M., Nilsson, A., Korhonen, K., Lodge, A., Lengyel, S.N. & Constable, C.G., 2015. GEOMAGIA50.v3: 1. General structure and modifications to the archeological and volcanic database, *Earth Planets Space,* **67,** 83–113.

Burlatskaya, S.P., Nachasova, I.E., Didenko, E.J. & Shelestun, N.K., 1986. *Archeomagnetic Determinations of Geomagnetic Field Elements of the USSR Academy of Sciences,* Soviet Geophysical Committee of the USRR Academy of Sciences.

Cai, S. *et al.*, 2016. New archaeomagnetic direction results from China and their constraints on palaeosecular variation of the geomagnetic field in Eastern Asia, *Geophys. J. Int.,* **207,** 1332–1342.

Cech, B., 2014. The production of *ferrum noricum* at Hüttenberg, Austria - the results of archaeological excavations carried out from 2003 to 2010 at the site Semlach/Eisner. in *Early Iron in Europe,* eds. Cech, B. & Rehren, T., édition monique mergoil.

Clark, A.J., Tarling, D.H. & Noel, M., 1988. Developments in archaeomagnetic dating in Britain, *J. Archaeol. Sci.,* **15,** 645–667.

Dunlop, D. & Özdemir, Ö., 1997. *Rock Magnetism, Fundamentals and Frontiers*. Cambridge University Press, Cambridge.

Fisher, R.A., 1953. Dispersion on a sphere, *Proc. R. Soc. London,* **A-127,** 295–305.

Gallet, Y., D'Andrea, M., Genevey, A., Pinnock, F., Le Goff, M. & Matthiae, P., 2014. Archaeomagnetism at Ebla (Tell Mardikh, Syria). New data on geomagnetic field intensity variations in the Near East during the Bronze Age, *J. Archaeol. Sci.,* **42,** 295–304.

Gassmann, G., Mathes, B. & Wieland, G., 2011. Vorläufiger Abschluss der montanarchäologischen Untersuchungen im Grösseltal bei Neuenbürg, *Arch. Ausgr. Baden-Württemberg,* **2010,** 112–117.

Gassmann, G. & Schäfer, A., 2014. Early iron production in Germany - a short review. in *Early Iron in Europe,* eds. Cech, B. & Rehren, T., édition monique mergoil.

Glaser, F., 1991. *Das frühchristliche Pilgerheigtum auf dem Hemmaberg,* Verlag des Geschichtsvereins Kärnten., Klagenfurt.

Goralczyk, P., 2006. Meyenburg. Die Baugeschichte des Schlosses im Überblick, *Brandenburgische Denkmalpflege,* **15,** 27–49.

Gutjahr, C., 2018. Faltikögerl, *Hengist - Best-of, Führer zu archäologischen Fundstellen und Baudenkmalen in der Region Hengist, Hengist-Magazin Sonderband ,* **1,** 50–53.

Hanesch, M., Stanjek, H. & Petersen, N., 2006. Thermomagnetic measurements soil iron minerals: the role of organic carbon, *Geophys. J. Int.,* **165,** 53–61.

Hervé, G., Chauvin, A. & Lanos, P., 2013. Geomagnetic field variations in Western Europe from 1500BC to 200AD. Part I: Directional secular variation curve, *Phys. Earth planet. Inter.,* **218,** 1–13.

Hervé, G., Schnepp, E., Chauvin, A., Lanos, P. & Nowaczyk, N., 2011. Archeomagnetic results on three First Iron Age salt-kilns from Moyenvic (France), *Geophys. J. Int.,* **185,** 144–156.

Hervé, G. *et al.*, 2017. Fast geomagnetic field intensity variations between 1400 and 400 BCE: New archaeointensity data from Germany, *Phys. Earth planet. Inter.,* **270,** 143–156.

Jackson, A., Jonkers, A.R.T. & Walker, M.R., 2000. Four centuries of geomagnetic secular variation from historical records, *Phil. Trans. R. Soc. Lond. A,* **358,** 957–990.

Jonkers, A.R.T., Jackson, A. & Murray, A., 2003. Four centuries of geomagnetic data from historical records, *Rev. Geophys.,* **41,** 1–74.

Jordanova, N., 2017. *Soil Magnetism, Applications in Pedology, Environmental Science and Agriculture*. Academic Press, London.

Kirschvink, J.L., 1980. The least squares line and plane and the analysis of paleomagnetic data, *Geophys. J. R. astr. Soc.,* **62,** 699–718.

Klemm, S., 2003. *Montanarchäologie der Eisenerzer Alpen, Steiermark*. Verlag der Österreichischen Akademie der Wissenschaften.

Klemm, S., 2004. Der prähistorische Kupferschmelzplatz S 1 in der Eisenerzer Ramsau (Steiermark). in *Alpenkupfer - Rame delli Alpiv*. eds. Weisgerber, G. & Goldenberg, G., Der Anschnitt, Beiheft 17, 189–198.

Klemm, S., 2006. Die Erforschung der prähistorischen Kupfergewinnung in den Eisenerzer Alpen 1955 - 2005, *Res montanarum, Zeitschrift des montanhistorischen Vereins,* **38,** Festschrift Gerhard Sperl, 26–36.

Klemm, S., Nelle, O., Grabner, M., Geihofer, D. & Schnepp, E., 2005. Interdisziplinäre Untersuchungen von Kohlenstätten aus Mittelalter und Neuzeit in der Eisenerzer Ramsau, Steiermark, *Archaeologia Austriaca,* **89,** 269–329, printed in 2007.

Klemm, S., Smidt, E., Tintner, J., Grabner, M., Jeitler, M., Arneitz, P. & Leonhardt, R., 2017. Möglichkeiten zur zeitlichen Einordnung von historischen Holzkohlemeilern – Eine interdisziplinäre Zusammenarbeit, *Beiträge zur Mittelalterarchäologie in Österreich,* **33,** 67–82.

Koenigsberger, J., 1936. Die Abhängigkeit der natürlichen remanenten Magnetisierung bei Eruptivgesteinen von deren Alter und Zusammensetzung, *Beitr. Angew. Geophys.,* **5,** 193–246.

Korte, M., Constable, C., Donadini, F. & Holme, R., 2011. Reconstructing the Holocene geomagnetic field, *Earth planet. Sci. Lett.,* **312,** 497–505.

Kostadinova-Avramova, M. & Kovacheva, M., 2013. The magnetic properties of baked clays and their implications for past geomagnetic field intensity determination, *Geophys. J. Int.,* **195,** 1534–1550.

Kovacheva, M., Chauvin, A., Jordanova, N., Lanos, P. & Karloukovski, V., 2009. Remanence anisotropy effect on the palaeointensity results obtained from various archaeological materials, excluding pottery, *Earth Planets Space,* **61,** 711–732.

Krenn, E., 2005. Die Ausgrabungen in Wörterberg 2004, in: *FACHGESPRÄCHE: Die Là Tene-Zeit und die römische Kaiserzeit im norisch-pannonischen Grenzgebiet, Grenzüberschreitende Tagung zwischen Österreich und Ungarn, ed.),* eds. Verein Lafnitztal Historik.

Krenn, E., 2007. Eine römerzeitliche Fundstelle an der Lafnitz Wörterberg, Bezirk Güssing, *Burgenländische Heimatblätter,* **69,** 189–199.

Kuhn, R., Pöppelmann, H., Puhle, M. & Weber, T., 2003. Wenn der Stein ins Rollen kommt, *Archäologie in Deutschland,* **6,** 8–12.

Lanos, P., 2004. Bayesian inference of calibration curves: application to archaeomagnetism. in *Tools for Constructing Chronologies, Crossing Disciplinary Boundaries*. eds. Buck, C.E. & Millard, A.R., Springer-Verlag.

Lanos, P., Le Goff, M., Kovacheva, M. & Schnepp, E., 2005. Hierarchical modelling of archaeomagnetic data and curve estimation by moving average technique, *Geophys. J. Int.,* **160,** 440–476.

Lanting, J.N. & Plicht, J.v.d., 2003. De 14C-chronologie van de Nederlandse pre- en protohistorie, IV: bronstijd en vroege ijzertijd, *Palaeohistoria,* **43/44**(2001/2002), 117–262.

McFadden, P.L., 1982. Rejection of palaeomagnetic observations, *Earth planet. Sci. Lett.,* **61,** 392–395.

McFadden, P.L. & Lowes, F.J., 1981. The discrimination of mean directions drawn from Fisher distributions, *Geophys. J.,* **67,** 19–33.

Müller, U. & Patzschke, R., 2006. Meyenburg. Die Ausgrabungen im Schloss. Ein Vorbericht, *Brandenburgische Denkmalpflege,* **15,** 51–56.

Neutzer, C., 2003. Archäologische Ausgrabungen im Vorfeld des Autobahnbaus der A 20, Abschnitt Brunn - Neubrandenburg, Grabungbericht: Glocksin, Landkreis Mecklenburg-Strelitz, Fpl. 15*51*, ed.),∧eds. Landesamt für Kultur und Denkmalpflege Mecklenburg-Vorpommern.

Nilsson, A., Suttie, N. & Hill, M., 2018. Short-term magnetic field variations from the post-depositional remanence of lake sediments, *Frontiers in Earth Science,* **6,** 39.

Pavón-Carrasco, F.J., Osete, M.L., Torta, J.M. & Santis, A.D., 2014. A geomagnetic field model for the Holocene based on archaeomagnetic and lava flow data, *Earth planet. Sci. Lett.,* **388** 98–109.

Poletti, W., Biggin, A.J., Trindade, R.I.F., Hartmann, G.A. & Terra-Nova, F., 2018. Continuous millennial decrease of the Earth's magnetic axial dipole, *Phys. Earth planet. Inter.,* **274,** 72–86.

Reimer, P.J. *et al.*, 2009. IntCal09 and Marine09 radiocarbon age calibration curves, 0–50,000 years cal BP, *Radiocarbon,* **51,** 1111–1150.

Risy, R. & Scherrer, P., 2005. *Municipium Aelium Cetium - Landeshauptstadt St. Pölten. Archäologische Grabungen und Forschungen 1999–2005*. Bischöfl. Ordinariat St. Pölten.

Schnepp, E., 2008a. Archäomagnetische Altersbestimmung der Kalkbrennöfen HaK 46 und 47. in *Archäologie auf Waldeshöhen. Eisenzeit, Mittelalter und Neuzeit auf der "Kalteiche" bei Haiger, Lahn-Dill-Kreis*. ed., Verse, F., Verlag Marie Leidorf GmbH.

Schnepp, E., 2008b. Archäomagnetische Datierung eines Kuppelofens im Braukohletagebau Jänschwalde. in *Ausgrabungen im Niederlausitzer Braunkohlenrevier, Arbeitberichte zur Bodendenkmalpflege 20*. ed., Schopper, F., Brandenburgisches Landesamt für Denkmalpflege und Archäologisches Landesmuseum.

Schnepp, E., 2010a. Archäomagnetische Datierung der Glasöfen am Füllenberg bei Altenbeken-Buke. in Landschaftsverband-Westfalen-Lippe (ed.), *Archäologie in Westfalen-Lippe 2009*. Beier & Beran.

Schnepp, E., 2010b. Archäomagnetische Datierung der Öfen auf der Grabung Damsdorf. in *Archäologische Studien zum Dorf der Ostsiedlungszeit. Die Wüstungen Miltendorf und Damsdorf in Brandenburg und das ländliche Siedlungswesen des 12. bis 15. Jahrhunderts in Ostmitteleuropa*. ed., Biermann, F., Brandenburgisches Landesamt für Denkmalpflege und Archäologisches Landesmuseum.

Schnepp, E., 2011a. Archäo-, Paläo- und Umweltmagnetik. in *Umweltarchäologie - Naturkatastrophen und Umweltwandel im archäologischen Befund. 3. Mitteldeutscher Archäologentag vom 07. bis 09. Oktober 2010 in Halle (Saale)*. eds. Bork, H.-R., Meller, H. & Gerlach, R., Tagungen des Landesmuseum für Vorgeschichte Halle, 6.

Schnepp, E., 2011b. Archäomagnetische Datierungen an Grabungsbefunden. in *Die Karnburg. Forschungen zu Kärntens Königspfalz 2006–2010*. eds. Dolenz, H. & Baur, C., Verlag des Landesmuseums für Kärnten.

Schnepp, E., 2015. Archäomagnetische Datierung: Möglichkeiten und Grenzen einer naturwissenschaftlichen Methode zur Altersbestimmung. in *23. Treffen der Archäologische Arbeitsgemeinschaft Ostbayern/West- und Südböhmen /Oberösterreich, Kostenz*. eds. Husty, L., Verlag Maria Leidorf.

Schnepp, E., 2016. Archäomagnetische Datierung von Befunden am "Kleinen Schmidtskopf" bei Elbingerode, Lkr. Harz. in *Frühmittelalterliche Eisengewinnung im Susenburger Revier bei Elbingerode Eisenverhüttung bei Elbingerode, mit Beiträgen von Elisabeth Schnepp und Monika Hellmund*. ed. Alper, G., Beier & Beran.

Schnepp, E., 2017. Archäomagnetische Datierungen auf der Grabung Semlach/Eisner bei Knappenberg (Kärnten), in *Die Produktion von Ferrum Noricum am Hüttenberger Erzberg. Die Ergebnisse der interdisziplinären Forschungen auf der FundstellenSemlach/Eisner in den Jahren 2006 - 2010,* ed. Cech, B., Unipressverlag.

Schnepp, E., 2018. Archäomagnetische Messungen an den Öfen der Talsiedlung von Thunau am Kamp (Niederösterreich), in *50 Jahre Archäologie in Thunau am Kamp. Festschrift für Herwig Friesinger,* pp. 281–288. eds Nowotny, E., Obenaus, M. & Uzunoglu-Obenaus, S., Archäologische Forschungen in Niederösterreich (AFNÖ) 5.

Schnepp, E. & Brüggler, M., 2016. Archaeomagnetic investigation of a Roman glass workshop in Goch-Asperden, Germany, *J. Arch. Sci.: Rep.,* **10,** 322–330.

Schnepp, E. & Lanos, P., 2005. Archaeomagnetic secular variation in Germany during the past 2500 years, *Geophys. J. Int.,* **163,** 479–490.

Schnepp, E. & Lanos, P., 2006. A preliminary secular variation reference curve for archaeomagnetic dating in Austria, *Geophys. J. Int.,* **166,** 91–96.

Schnepp, E., Lanos, P. & Chauvin, A., 2009. Geomagnetic paleointensity between 1300 and 1750 A.D. derived from a bread oven floor sequence in Lübeck, Germany, *Geochem. Geophys. Geosyst.,* **10,** Q08003, doi:10.1029/2009GC002470.

Schnepp, E., Leonhardt, R., Korte, M. & Klett-Drechsel, J., 2016. Validity of archaeomagnetic field recording: an experimental pottery kiln at Coppengrave, Germany, *Geophys. J. Int.,* **205,** 622–635.

Schnepp, E., Obenaus, M. & Lanos, P., 2015. Posterior archaeomagnetic dating: an example from the early Medieval site Thunau am Kamp, Austria, *J. Arch. Sci. Rep.,* **2,** 688–698.

Schnepp, E., Pucher, R., Goedicke, C., Manzano, A., Müller, U. & Lanos, P., 2003. Paleomagnetic directions and TL dating from a bread oven-floor sequence in Lübeck (Germany): a record of 450 years of geomagnetic secular variation, *J. geophys. Res.,* **108**(B2), 1–14, doi:10.1029/2002JB001975.

Schnepp, E., Pucher, R., Reinders, J., Hambach, U., Soffel, H.C. & Hedley, I., 2004. A German catalogue of archaeomagnetic data, *Geophys. J. Int.,* **157,** 64–78.

Schnepp, E., Scholger, R., Mauritsch, H., Lanos, P. & Rolf, C., 2006. New archaeomagnetic data from Austria and Germany,in *Poster EGU06-A-10136, EUG General Assembly,* April 2nd to 7th.

Schnepp, E., Worm, K. & Scholger, R., 2008. Improved sampling techniques for baked clay and soft sediments, *Phys. Chem. Earth, Parts A/B/C,* **33,** 407–413.

Shaar, R., Tauxe, L., Ron, H., Ebert, Y., Zuckerman, S., Finkelstein, I. & Agnon, A., 2016. Large geomagnetic field anomalies revealed in Bronze and Iron age archaeomagentic data from tel Megiddo and tel Hazor, Israel, *Earth planet. Sci. Lett.,* **442,** 173–185.

Steinmetz, W.-D., 2008. Die archäologischen Ausgrabungen auf dem Burgwall von Isingerode 2006–2008, *Informationen und Berichte, Braunschweigisches Landesmuseum,* **2/2008,** 3–49.

Strahl, E., 2004. Ein Haus für Mensch und Tier, *Archäologie in Deutschland,* **2,** 26–27.

Strahl, E., 2005. Die jungbronzezeitliche Siedlung Rodenkirchen - Hahnenknooper Mühle, Ldkr. Wesermarsch – Erste Bauern in der deutschen Marsc,in *Kulturlandschaft Marsch. Natur, Geschichte, Gegenwart,* eds Endlich, C. & Kremer, P., Schriftenreihe des Landesmuseums für Natur und Mensch.

Strahl, E., 2007. Die Anfänge der Besiedlung der deutschen Marsch - Die spätbronzezeitliche Siedlung Rodenkirchen - Hahnenknooper Mühle, Ldkr. Wesermarsch. Abschlußbericht zum Forschungsvorhaben STR 494/1-7*1 - 99*, Niedersächsisches Institut für historische Küstenforschung.

Szameit, E., 2015. 50 Jahre Ausgrabungen in Gars-Thunau. Anmerkungen zu einem immer noch aktuellen archäologischen Großprojekt, *Archäologie Österreichs,* **26,** 2–8.

Tarling, D.H., 1971. *Principles and Applications of Palaeomagnetism*. Chapman and Hall Ltd.

Tarling, D.H. & Dobson, M.J., 1995. Archaeomagnetism: an error assessment of fired material observations in the British directional database, *J. Geomagn. Geoelectr.,* **47,** 5–18.

Tema, E., Hedley, I. & Lanos, P., 2006. Archaeomagnetism in italy: a compilation of data including new results and a preliminary Italian Secular Variation curve, *Geophys. J. Int.,* **167,** 1160–1171.

Thellier, E., 1938. Sur L'aimantation des terres cuites et ses applications géophysiques, *Ann. I. P. G. Paris,* **16,** 157–302.

Thellier, E. & Thellier, O., 1944. Recherches géomagnetiques sur des coulées volcaniques d'Auvergne, *Ann. Geophys.,* **1,** 37–52.

Thellier, E. 1981. Sur la direction du champ magnétique terrestre, en France, durant les deux derniers millénaires, *Phys. Earth planet. Inter.,* **27,** 1–7.

Trapanese, A., Batt, C.M. & Schnepp, E., 2008. Sampling methods in archaeomagnetic dating: a comparison using case studies from Wörterberg, Eisenerz and Gams Valley (Austria), *Phys. Chem. Earth,* **33,** 414–426.

Verse, F., 2008. *Archäologie auf Waldeshöhen. Eisenzeit, Mittelalter und Neuzeit auf der "Kalteiche" bei Haiger, Lahn-Dill-Kreis*. Verlag Marie Leidorf GmbH.

7 SUPPORTING INFORMATION

Supplementary data are available at *GJI* online.

SupplementaryMaterialsA.doc
SupplementaryMaterialsA.zip
SupplementaryMaterialsB.doc
SupplementaryMaterialsC.doc

Please note: Oxford University Press is not responsible for the content or functionality of any supporting materials supplied by the authors. Any queries (other than missing material) should be directed to the corresponding author for the paper.